

This is an Open Access document downloaded from ORCA, Cardiff University's institutional repository:<https://orca.cardiff.ac.uk/id/eprint/126675/>

This is the author's version of a work that was submitted to / accepted for publication.

Citation for final published version:

Muhammadsharif, Fahmi F., Hashim, Suhairul, Hameed, Shilan S., Ghoshal, S.K., Abdullah, Isam K., Macdonald, J.E. and Yahya, Mohd Y. 2019. Brent's algorithm based new computational approach for accurate determination of single-diode model parameters to simulate solar cells and modules. *Solar Energy* 193 , pp. 782-798. 10.1016/j.solener.2019.09.096

Publishers page: <http://dx.doi.org/10.1016/j.solener.2019.09.096>

Please note:

Changes made as a result of publishing processes such as copy-editing, formatting and page numbers may not be reflected in this version. For the definitive version of this publication, please refer to the published source. You are advised to consult the publisher's version if you wish to cite this paper.

This version is being made available in accordance with publisher policies. See <http://orca.cf.ac.uk/policies.html> for usage policies. Copyright and moral rights for publications made available in ORCA are retained by the copyright holders.



Brent's algorithm based new computational approach for accurate determination of single-diode model parameters to simulate solar cells and modules

Fahmi F. Muhammadsharif^{1,2,*}, Suhairul Hashim^{1,3}, Shilan S. Hameed⁴, S. K. Ghoshal¹, Isam K. Abdullah⁵, J. E. Macdonald⁶, Mohd Y. Yahya⁷

(1) Department of Physics, Faculty of Science, Universiti Teknologi Malaysia (UTM), 81310 Skudai, Johor, Malaysia

(2) Department of Physics, Faculty of Science and Health, Koya University, 44023 Koya, Kurdistan Region - F.R., Iraq

(3) Centre for Sustainable Nanomaterials (CSNano), Ibnu Sina Institute for Scientific and Industrial Research (ISI-SIR), Universiti Teknologi Malaysia (UTM), 81310 Skudai, Johor, Malaysia

(4) Directorate of Information Technology, Koya University, 44023 Koya, Kurdistan Region -F.R., Iraq

(5) Department of Physics, Salahaddin University, 44001 Erbil, Kurdistan Region-F.R., Iraq

(6) School of Physics and Astronomy, Cardiff University, Cardiff CF24 3AA, UK

(7) Center for Advanced Composite Materials (CACM), Institute for Vehicle Systems & Engineering, Faculty of Mechanical Engineering, Universiti Teknologi Malaysia, 81310 Skudai, Johor, Malaysia

* Corresponding author's email:

fahmi.fariq@koyauniversity.org

Tel.: +964-7501168841

Abstract

Simulated current-voltage (I - V) characteristics of photovoltaic (PV) cells and modules are significant for the performance assessment, design and quality control, which are decided by the accurate determination of the intrinsic parameters of the devices. Commonly, a single-diode model is utilized to extract these parameters such as the ideality factor (n), series resistance (R_s), shunt resistance (R_{sh}), saturation current (I_o) and photo-generated current (I_l). Driven by this idea, a new mathematical manipulation was performed on the single-diode equation that yielded a non-linear formula of R_s . Later, Brent's algorithm was used to precisely estimate R_s at every fine-tuned point of n , thereby all other parameters were determined. The set of parameters that provided the lowest root mean square error (RMSE) between the experimental and simulated I - V data were chosen to be optimum. The proposed Brent's algorithm (BA) was shown outperform several recently reported computational and

38 heuristic algorithms that were exploited to mine the single-diode model parameters for solar
39 cells and modules with varied device temperatures and solar irradiation conditions.

40

41 **Keywords:** Solar cells and modules, Parameters extraction, Brent's algorithm, *I-V*
42 simulation, sensitivity analysis.

43

44 **Abbreviations:**

45 ABC: Artificial Bee Colony

46 ABSO: Artificial Bee Swarm Optimization

47 ADA: Adaptive Differential Algorithm

48 BA: Brent's Algorithm

49 BMO: Bird Mating Optimizer

50 CPSO: Chaos Particle Swarm Algorithm

51 CSO: Cat Swarm Optimization

52 CWOA: Chaotic Whale Optimization Algorithm

53 DET: Differential Evolution Technique

54 EHA-NMS: Eagle-based Hybrid Adaptive Nelder-Mead Simplex Algorithm

55 ELPSO: Enhanced Leader Particle Swarm Optimization

56 ER-WCA: Evaporation Rate-based Water Cycle Algorithm

57 GA: Genetic Algorithm

58 GGHS: Grouping-based Global Harmony Search

59 GOTLBO: Generalized Oppositional Teaching Learning Based Optimization

60 HFAPS: Hybrid Firefly and Pattern Search Algorithm

61 HS: Harmony Search

62 IGHS: Innovative Global Harmony Search

- 63 ILCOA: Improved Lozi Map based Chaotic Optimization Algorithm
- 64 ISCE: Improved Shuffled Complex Evolution
- 65 MABC: Modified Artificial Bee Colony
- 66 MAE: Mean of Absolute Error
- 67 MPCOA: Mutative-scale Parallel Chaos Optimization Algorithm
- 68 NM-MPSO: Nelder-Mead and Modified Particle Swarm Optimization
- 69 PCE: Population Classification Evolution
- 70 PGJAYA: Performance Guided JAYA
- 71 PS: pattern search
- 72 PSO: particle swarm optimization
- 73 R_{cr}-IJADE: Ranking-based Improved Adaptive Differential Evolution
- 74 RMSE: Root Mean Squared Error
- 75 SA: Simulated Annealing
- 76 SAE: Summation of Absolute Error
- 77 STLBO: simplified teaching-learning based optimization
- 78
- 79 **Nomenclature:**
- 80 I_o : saturation current
- 81 I_l : photo-generated current
- 82 k_B : Boltzmann's constant (1.381×10^{-23} J/K)
- 83 n : ideality factor
- 84 q : electron charge (1.602×10^{-19} C)
- 85 R_{sh} : shunt resistance
- 86 R_s : series resistance
- 87 T : temperature in Kelvin

88

89 **1. Introduction**

90 PV technologies are exploited to convert solar energy into electricity by means of
91 solar cells and modules comprising various architectural designs and active materials (Li et
92 al., 2007; McEvoy et al., 2012; Muhammad and Sulaiman, 2018; Muhammad, Fahmi F et al.,
93 2017; Otte et al., 2006). The easy installation and low maintenance costs of solar energy
94 derived electricity compared to other energy sources make PV technology more convenient
95 and effective. Various factors that affect the performance of PV devices include temperature,
96 solar insolation and aging (Ahmad et al., 2017; Meneses-Rodríguez et al., 2005; Muhammad
97 et al., 2018). Essentially, these factors modify the intrinsic parameters of solar cells and
98 modules, thereby reducing the cell efficiency. Therefore, it is important to model and analyse
99 the current-voltage (*I-V*) characteristics of these devices under diverse operational conditions
100 (Muhammad, Fahmi F. et al., 2017; Xiao et al., 2017).

101 Over the years, single-diode and double-diode models have been widely studied to
102 mimic the *I-V* characteristics (Humada et al., 2016; Muhammad, Fahmi F. et al., 2017;
103 Villalva, M. G. et al., 2009), wherein the real-world PV behaviour of solar cells and modules
104 have been simulated. The single-diode model has been proven to be accurate approach for the
105 PV devices in terms of simplicity and fast implementation response (Kumar and Kumar,
106 2017; Orioli and Di Gangi, 2016; Tong and Pora, 2016). This model is represented by an
107 equivalent circuit which is composed of a constant current source connected to an ideal diode
108 in parallel with a shunt resistance driving an external load through a series resistance (Fig.
109 1(b)).

110 For the purpose of performance assessment, simulation, design, and quality control,
111 the precise estimation of the solar cells and modules parameters values are significant
112 (Maouhoub, 2018a). Besides, these parameters can be used effectively to predict the energy

113 yield (Müller et al., 2016), to develop algorithm for maximum power point trackers (MPPTs)
114 (Tajuddin et al., 2015; Verma et al., 2016), to develop plug-in hybrid electric vehicles
115 (PHEVs) (Hu et al., 2016), to address the degradation and aging issues in PV devices,
116 (Domanski et al., 2018; Neubauer et al., 2019), and to understand the outdoor operation of
117 PV cells and panels at various environmental conditions (Gaglia et al., 2017). Generally, the
118 manufacturers of PV devices provide a datasheet that includes open circuit voltage (V_{oc}),
119 short circuit current (I_{sc}), maximum rated power (P_m), voltage and current temperature
120 coefficients at standard test condition (STC). However, in the real-world situation the PV
121 devices do not always operate at this standard condition. Often, it is difficult to carry out a
122 steady practical I - V measurement over a long-time span and under different outdoor
123 situations. Therefore, it is vital to extract the intrinsic parameters of these devices first before
124 utilizing them in a viable model that is capable of well simulating the I - V curve of solar cells
125 and modules at every stage of their utilization and under varied environmental conditions.

126 Sequentially, various analytical and computational approaches as well as combined
127 strategies were adopted. In the analytical methods, the mathematical equations are
128 manipulated in a way that few characteristic I - V points (e.g., V_{oc} , I_{sc} , V_m and I_m) that are
129 provided in the manufacturer's datasheet can be utilized to extract the PV cells and modules
130 parameters (Louzazni and Aroudam, 2015; Park and Choi, 2015; Rasool et al., 2017;
131 Villalva, Marcelo Gradella et al., 2009). Despite a simple implementation, analytical methods
132 neither guarantee the high accuracy nor the realistic estimate of the PV cells and modules
133 parameters (Pindado and Cubas, 2017; Senturk and Eke, 2017; Yadir et al., 2009; Yildiran
134 and Tacer, 2016). This is because only limited regions of data from the I - V curve are
135 considered, resulting in high discrepancies between the simulated and measured I - V curve.
136 Alternatively, higher accuracy can be achieved at the expense of increased computational
137 complexity provided the entire I - V data is incorporated into the proposed mathematical

138 equations. These derived set of equations are solved by deterministic computational methods
139 including Newton-Raphson, Levenberg–Marquardt, polynomial curve fitting, Lambert-W
140 function and conductivity approach (Chegaar et al., 2001; Chen et al., 2011;
141 Easwarakhanthan et al., 1986; Ma et al., 2014). However, these methods are based on
142 gradient numerical optimization, wherein the proposed equation must be continuous and
143 differentiable over the given interval in order to get the best approximate solution.

144 Interestingly, stochastic computational optimization based on evolutionary and
145 heuristic algorithms received considerable attention for their capacity of handling nonlinear
146 equations and global search pattern. For instance, differential evolution (DE) technique
147 (Gong and Cai, 2013; Ishaque and Salam, 2011), bird mating optimizer (BMO) (Askarzadeh
148 and dos Santos Coelho, 2015; Askarzadeh and Rezazadeh, 2013b, c), genetic algorithm (GA)
149 (Jervase et al., 2001; Zagrouba et al., 2010), artificial bee colony (ABC) (Oliva et al., 2014)
150 and particle swarm optimization (PSO) (Ye et al., 2009; Yeh, 2009) were successfully
151 utilized to estimate the parameters of PV cells and modules. Basically, these algorithms work
152 on a random selection of the intended parameters simultaneously within a large solution
153 space, ultimately leading to high computational cost and reduced stability. On top, the
154 solution may easily get stuck into the local optimum when the dimension of the objective
155 function is large (Gao et al., 2018). Very recently, researchers have made attempts to better
156 compensate for the limitations of stochastic computational techniques through the
157 establishment of alternative algorithms and internal parametric modifications. Examples of
158 these approaches are PSO with binary constraints (Bana and Saini, 2017), guaranteed
159 convergence PSO (Nunes et al., 2018), improved chaotic whale optimization algorithm
160 (Oliva et al., 2017), improved shuffled complex evolution algorithm (Gao et al., 2018) and
161 hybrid firefly algorithm with pattern search algorithm (HFAPS) (Beigi and Maroosi, 2018).
162 Additionally, with the aim of combining the simplicity of analytical methods and efficiency

163 of computational techniques various hybrid approaches were adopted to estimate the PV cells
164 and modules parameters (Chin et al., 2015; Cubas et al., 2014a; Kumar and Kumar, 2017;
165 Maouhoub, 2018b).

166 It is known that the performance and accuracy of the techniques used to estimate the
167 single-diode parameters are usually limited by the complexity of their implementation and
168 reproducibility as well as by the methodology of computational approaches that affect the
169 simulated I - V curve which deviates from the experimental one. It is because the I - V
170 characteristic is highly sensitive to the values of ideality factor and series resistance
171 (Muhammad, Fahmi F. et al., 2017). Thus, special attention must be paid to the initial
172 estimation of the ideality factor and series resistance while implementing the derived
173 equations. To surmount this issue, a new mathematical manipulation is proposed wherein an
174 implicit equation of series resistance (R_s) is initially derived. Later, Brent's Algorithm (BA)
175 (Brent, 2013) is used to determine the roots of the non-linear equations with assured
176 convergence. This could accurately estimate R_s at every fine-tuned point of n . Finally,
177 complete set of values of R_s and n were considered to extract the rest of the parameters. The
178 set of parameters which provided the lowest root mean square error (RMSE) between the
179 experimental and simulated I - V data were selected as the optimum solution. The proposed
180 BA was deployed via MATLAB programming code to build a user-friendly software
181 application which could automatically perform the process of parameters extraction.

182 Simple implementation of this technique via the utilization of few viable equations
183 and high accuracy of the simulated I - V compared to that of the experimental ones at various
184 environmental conditions can be featured as two main contributions of the current work. The
185 proposed method required a set of I - V data without the need of providing PV parameters
186 manually. The method itself used the extrapolation fitting to estimate the PV parameters prior
187 to the initialization. The rest of the paper describes the methodology of the mathematical

188 manipulations and the implementation of BA used to extract accurately the parameters and I -
189 V curve. Subsequently, the method was validated on both of solar cells and modules operated
190 under different device temperatures and solar irradiations. Finally, the main conclusions of
191 the research were drawn.

192

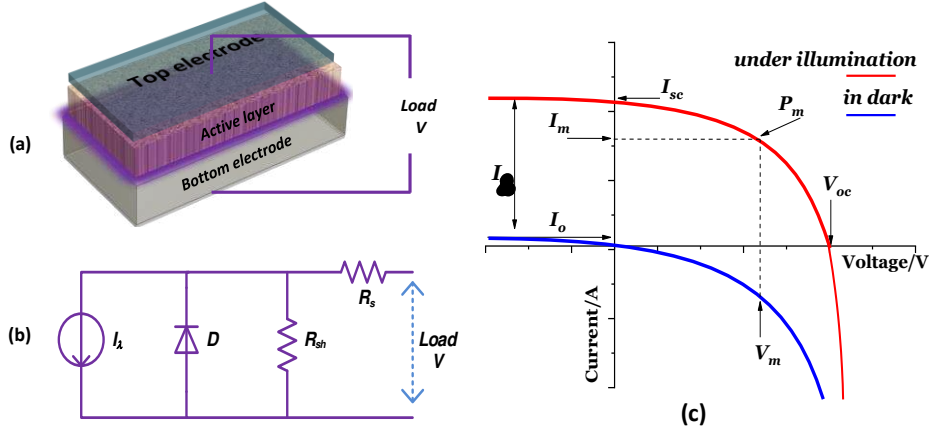
193 **2. Methodology**

194 **2.1. Mathematical Formalism**

195 Figs. 1(a-c) show the structure of a typical photovoltaic device, its equivalent circuit
196 and standard I - V characteristics under dark and illumination, respectively. The light activated
197 current source (I_λ) defines the amount of current generated in the cell when exposed to
198 sunlight energy. The net current in the connected load determines the final characteristic
199 current of the device, which is represented by.

$$200 \quad I = I_\lambda - I_o \left[\exp\left(\frac{V + IR_s}{nV_t}\right) - 1 \right] - \frac{(V + IR_s)}{R_{sh}} \quad (1)$$

201 where n is the ideality factor of the solar cell signifying the charge transport efficiency of the
202 device, I_o is the saturation (generation) current of the diode under dark conditions, V_t is the
203 thermal voltage represented by $k_B T/q$, k_B is the Boltzmann's constant, T is the temperature
204 in Kelvin, q is the elementary charge and R_s and R_{sh} are the respective series and shunt
205 resistance. For a PV module, $(V + IR_s) = (V/N_s + IR_s)$ since PV module is composed of N_s
206 series connected cells. Consequently, the denominator of the exponent part in the equation is
207 involved with N_s . Thus, during the numerical iterations, $(N_s \times n)$ should be considered instead
208 of n . The validity of single-diode model is dependent on the applicability of the principle of
209 superposition, whereby the effect of illumination is simply to displace the current by an
210 amount equal to I_λ everywhere along the I - V curve and whereby all other terms in Eq. (1)
211 retain their unilluminated and/or unbiased values (Del Cueto and Rummel, 2005).



212

213 **Fig. 1. A prototype structure of PV cells (a), the equivalent circuit used to simulate I - V curve of**
 214 **PV cells based on single-diode model (b) and their standard I - V characteristics (c).**

215

216 Based on the I - V characteristic curves shown in Fig. 1(c), three boundary conditions
 217 can be considered at the points of open circuit voltage (V_{oc}), short circuit current (I_{sc}) and
 218 maximum power (P_m) such that Eq. (1) takes the form (Chaibi et al., 2018):

$$219 \quad 0 = I_\lambda + I_o - I_o \exp\left(\frac{V_{oc}}{nV_t}\right) - \frac{V_{oc}}{R_{sh}} \quad (2)$$

$$220 \quad I_{sc} = I_\lambda + I_o - I_o \exp\left(\frac{R_s I_{sc}}{nV_t}\right) - \frac{R_s I_{sc}}{R_{sh}} \quad (3)$$

$$221 \quad I_m = I_\lambda + I_o - I_o \exp\left(\frac{R_s I_m + V_m}{nV_t}\right) - \frac{R_s I_m}{R_{sh}} - \frac{V_m}{R_{sh}} \quad (4)$$

222 Subtracting Eq. (2) from Eq. (3), the saturation current (I_o) was obtained:

$$223 \quad I_o = \frac{I_{sc} - \frac{V_{oc}}{R_{sh}} + \frac{R_s}{R_{sh}} I_{sc}}{\exp\left(\frac{V_{oc}}{nV_t}\right) - \exp\left(\frac{R_s I_{sc}}{nV_t}\right)} \quad (5)$$

224 By neglecting $\exp\left(\frac{R_s I_{sc}}{nV_t}\right)$ one can simplify the calculations wherein corresponding Eq. (3)

225 and Eq. (5) reduced to:

$$226 \quad I_{sc} = I_\lambda + I_o - \frac{R_s I_{sc}}{R_{sh}} \quad (6)$$

$$227 \quad I_o = \frac{I_{sc} - \frac{V_{oc}}{R_{sh}} + \frac{R_s}{R_{sh}} I_{sc}}{\exp\left(\frac{V_{oc}}{nV_t}\right)} \quad (7)$$

228 Using Eq. (6) and Eq. (4) one achieves:

$$229 \quad I_\lambda + I_o = I_{sc} + \frac{R_s I_{sc}}{R_{sh}} = I_m + I_o \exp\left(\frac{R_s I_m + V_m}{nV_t}\right) + \frac{R_s I_m}{R_{sh}} + \frac{V_m}{R_{sh}} \quad (8)$$

230 By substituting Eq. (7) into Eq. (8) and solving for R_{sh} one gets:

$$231 \quad R_{sh} = \frac{R_s I_{sc} A - V_{oc} A - R_s I_{sc} + R_s I_m + V_m}{I_{sc} - I_m - I_{sc} A} \quad (9)$$

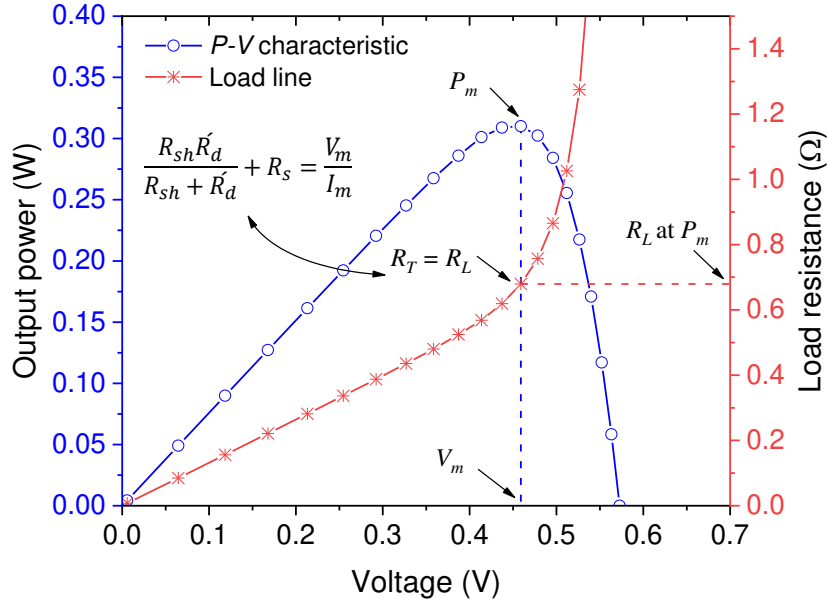
232 where $A = \exp\left(\frac{R_s I_m + V_m}{nV_t}\right)$. Another explicit relation can also be derived for R_{sh} by applying a
 233 boundary condition at the maximum power point (P_m) on the power-voltage (P - V) curve as
 234 depicted in Fig. 2. When a solar cell operates at P_m , maximum power is delivered to the
 235 external load. In this situation, the total internal resistance (R_T) of the solar cell (equivalent
 236 circuit) corresponds to the resistance of the external load (R_L):

$$237 \quad R_T = R_L = \frac{V_m}{I_m} \quad (10)$$

238 Based on the equivalent circuit, Eq. (10) can be applicable at the point of P_m ($I_m \times V_m$)
 239 regardless of the temperature and irradiation conditions as long as the load resistance is
 240 exactly matched to the total internal resistance:

$$241 \quad \frac{R_{sh} \check{R}_d}{R_{sh} + \check{R}_d} + R_s = \frac{V_m}{I_m} \quad (11)$$

242 where \check{R}_d is the dynamic resistance of the diode at P_m and it is determined from the first
 243 derivative of the diode voltage with respect to its current. A non-linear load line is noticeable
 244 in Fig. 2, which arises due to the nonlinear increase in the potential difference on R_L with the
 245 increase of R_L value across the PV devices.



246

247 **Fig. 2. P - V curve and load line for a typical solar cell, revealing maximum power**

248

delivery to the load at V_m .

249

250

251
$$R'_d = \left. \frac{dV_D}{dI_D} \right|_{P_m} = \frac{nV_t}{I_o \exp\left(\frac{R_s I_m + V_m}{nV_t}\right)} \quad (12)$$

252 Substituting Eq. (12) into Eq. (11) and performing few mathematical manipulations one

253 obtains:

254
$$I_o \exp\left(\frac{R_s I_m + V_m}{nV_t}\right) = \frac{nV_t \left(I_m - \frac{V_m}{R_{sh}} + \frac{R_s I_m}{R_{sh}}\right)}{V_m - R_s I_m} \quad (13)$$

255 Similarly, by subtracting Eq. (2) from Eq. (4) and combining Eq. (7) one gets:

256
$$I_o \exp\left(\frac{R_s I_m + V_m}{nV_t}\right) = I_{sc} - I_m + \frac{R_s}{R_{sh}} (I_{sc} - I_m) - \frac{V_m}{R_{sh}} \quad (14)$$

257 From Eq. (13) and Eq. (14) one achieves the second explicit form of R_{sh} given by:

258
$$R_{sh} = \frac{V_m^2 + R_s^2 (I_{sc} I_m - I_m^2) + R_s (nV_t I_m - I_{sc} V_m) - nV_t V_m}{R_s (I_m^2 - I_{sc} I_m) + V_m (I_{sc} - I_m) - nV_t I_m} \quad (15)$$

259 By combining Eq. (9) and Eq. (15) it is possible to derive a stand-alone implicit relation for
 260 R_s represented by:

$$261 \quad R_s = \frac{V_{oc}V_m(I_{sc} - I_m) + nV_t(I_{sc}V_m - I_mV_{oc}) - V_m^2I_{sc} + \frac{nV_tV_m(2I_m - I_{sc})}{A}}{I_{sc}I_m(V_{oc} - V_m) - I_m^2V_{oc}} \quad (16)$$

262 To predict the accuracy of the proposed method and to derive the cost function, summation of
 263 absolute error (SAE), mean of absolute error (MAE) and root mean squared error (RMSE)
 264 were calculated via the respective relations:

$$265 \quad SAE = \sum_{i=1}^k |I_i^{meas} - I_i^{sim}| \quad (17)$$

$$266 \quad MAE = \frac{1}{k} \sum_{i=1}^k |(I_i^{meas} - I_i^{sim})| \quad (18)$$

$$267 \quad RMSE = \sqrt{\frac{1}{k} \sum_{i=1}^k (I_i^{meas} - I_i^{sim})^2} \quad (19)$$

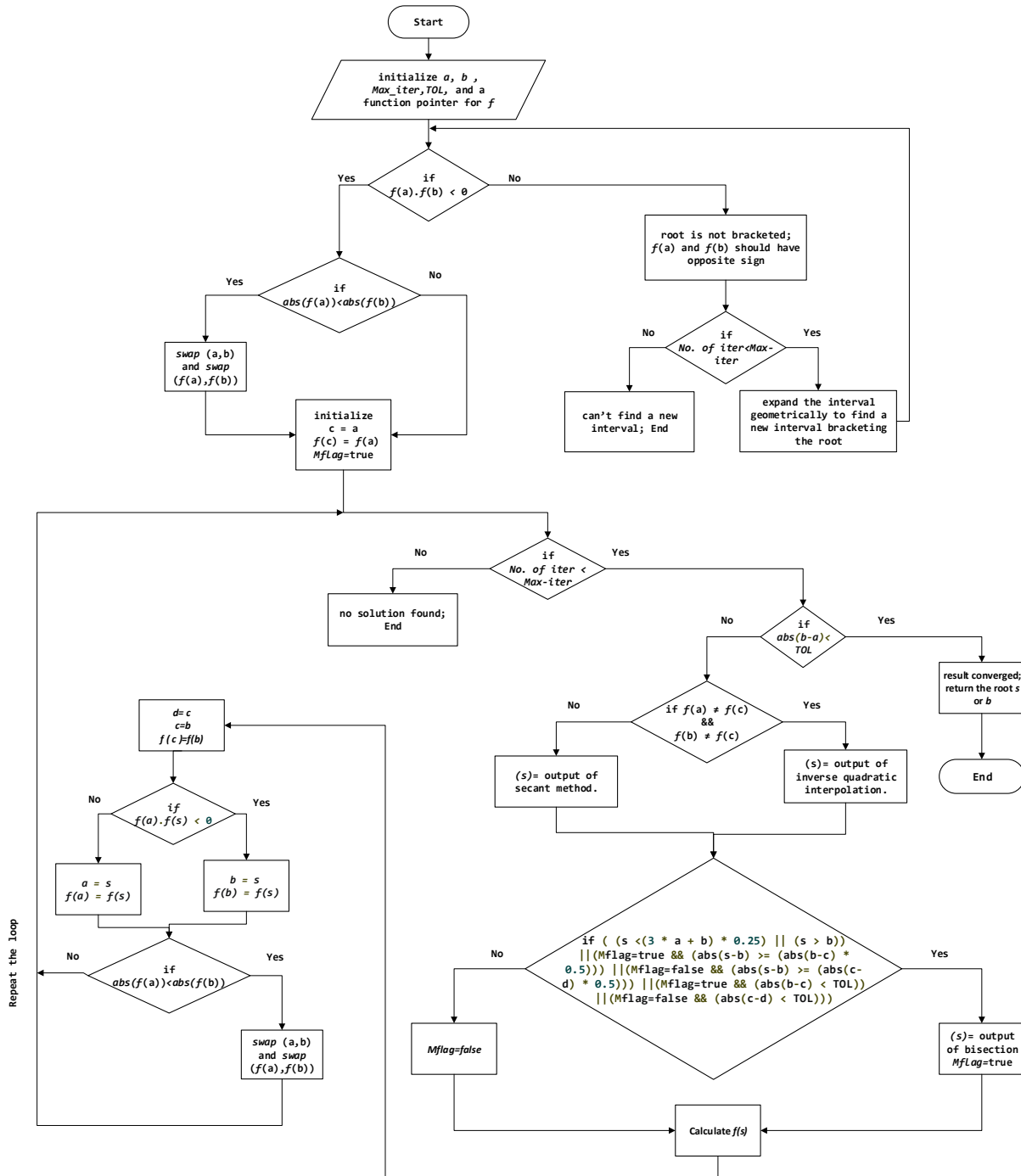
268 where k is the number of elements in the measured I - V set, I_i^{meas} and I_i^{sim} are the i^{th}
 269 measured and simulated current, respectively.

270

271 **2.2. Brent's Algorithm**

272 Brent's algorithm (BA) is a root-finding algorithm combining the inverse quadratic
 273 interpolation and methods of bisection as well as secant. It often uses the potentially fast-
 274 converging secant method or inverse quadratic interpolation, sometimes relies on the more
 275 robust bisection method if necessary. Therefore, BA has been purposely built to get benefit
 276 from the efficiency of the bisection method and low computational cost of the secant or
 277 inverse quadratic interpolation techniques. Fig. 3 illustrates a flowchart of BA used to find
 278 the zero of a function through sign changes in a given interval. In the present work, BA was
 279 successfully utilized to solve Eq. (16) for extracting the PV parameters and performing I - V

280 simulation. BA is guaranteed to converge for any function in a reasonable number of steps
 281 (Brent, 1971). BA can be used by means of *fzero* command in MATLAB, which is dedicated
 282 to find the zero of a function of single variable denoted by x based on a user-supplied initial
 283 guessed value x_0 (Magrab et al., 2007).

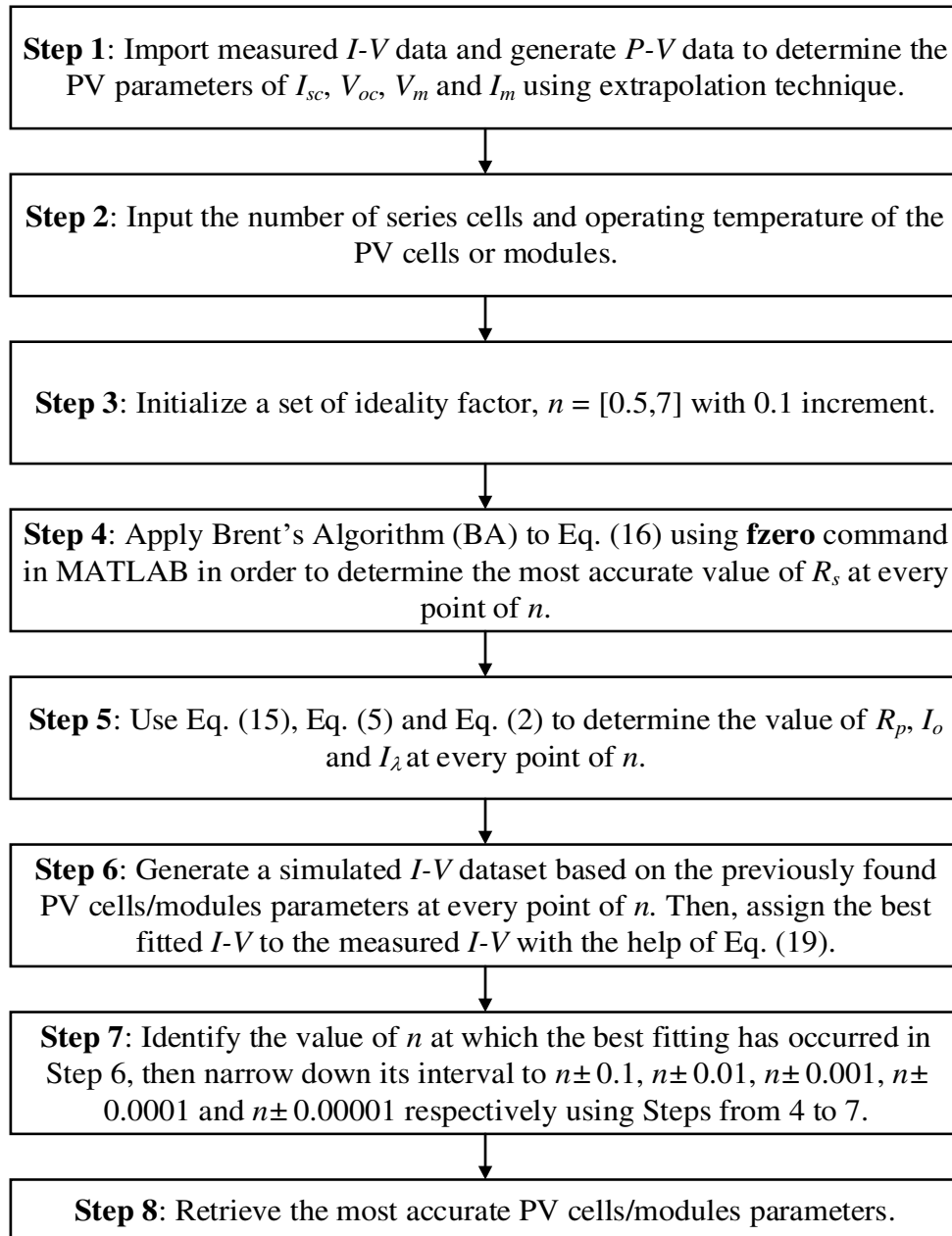


284
 285 **Fig. 3. Flowchart of Brent's algorithm used for efficient extraction of solar cells and**
 286 **modules parameters.**

287

288 **2.3. Implementation Procedure**

289 The implementation steps for solar cells and modules parameters extraction using the
290 proposed BA is presented in Fig. 4. First, the PV parameters (V_m , I_m , V_{oc} and I_{sc}) were
291 computed from the given I - V data using polynomial, exponential and polynomial curve
292 fittings around the points where P_m , I_{sc} and V_{oc} are located, respectively. Then, a set of n was
293 generated in the selected range of 0.5 to 7. Such choice guaranteed an accurate extraction of n
294 for almost every kind of solar cells and modules because some devices display relatively high
295 n . In each iteration, one value of n was chosen and Eq. (16) was solved to determine the most
296 accurate value of R_s using BA (see Fig. 3). Meanwhile, Eq. (15), Eq. (5) and Eq. (2) were
297 respectively used to estimate the value of R_{sh} , I_o and I_λ . Next, the extracted parameters from
298 every iteration were used to produce a bunch of simulated I - V curve. Finally, the set of
299 parameters which belonged to the simulated I - V curve presented the minimum cost function,
300 implying lowest RMSE between the measured and simulated I - V data, was chosen as the best
301 solution.



302

303

Fig. 4. Implementation steps for determining accurately the values of PV cells and modules parameters using BA to estimate the R_s .

304

305

306 3. Results and Discussion

307

Validation and assessment of the proposed BA was performed on eight different PV

308

devices (four PV cells and six PV modules) at different device temperatures and solar

309

irradiations. Consequently, the extracted PV cells and modules parameters were recorded and

310

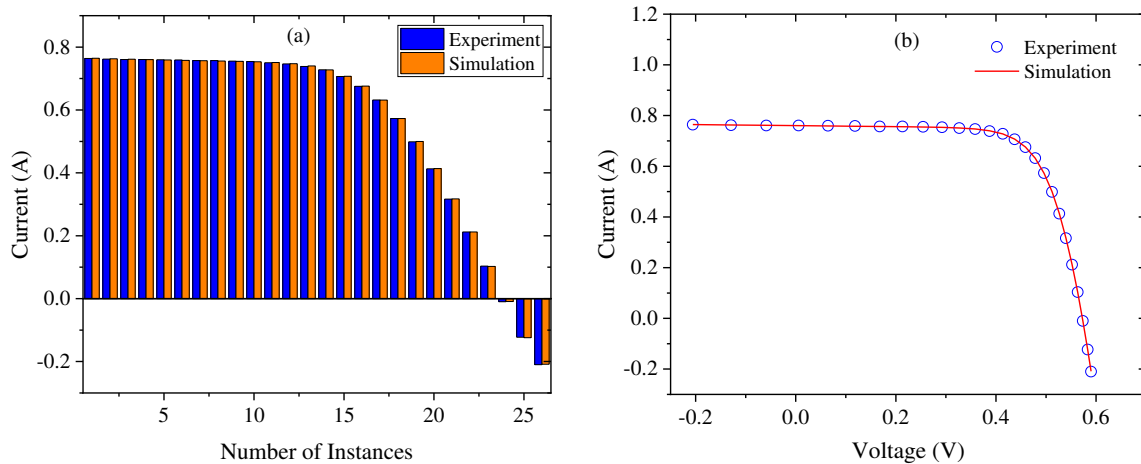
utilized to generate simulated I - V data for each type of the device. The correctness and

311 robustness of the proposed method was tested by comparing with the existing art of the
 312 techniques reported in the literature.

313

314 3.1 Validation on PV Cells

315 The validation and accuracy of the proposed BA was performed on two different solar
 316 cells such as R.T.C. France silicon and PVM 752 GaAs. The measured $I-V$ data for R.T.C.
 317 France solar cell with a 57 mm-diameter operating at cell temperature (T) of 33 °C and
 318 irradiation of 1000 W/m² was selected (Easwarakhanthan et al., 1986). Meanwhile, the PVM
 319 752 GaAs thin film solar cell was operated at 25 °C and irradiation of 1000 W/m², wherein
 320 the measured $I-V$ data was obtained (Jordehi, 2018). The BA based results for R.T.C. France
 321 single-crystalline solar cell are shown in Fig. 5, while the measured and calculated $I-V$ dataset
 322 is provided as Appendix A. Clearly, the simulated currents agreed very good well with the
 323 experimental ones. Fig. 5(a) showed that the proposed method is more sensitive to the PV
 324 parameters of V_m and I_m , where the simulated currents were more deviated from that of the
 325 measured currents around P_m . This can be ascribed to the effect of polynomial fitting which
 326 was used to extract the value of V_m and I_m from the experimental $I-V$ data. Besides, Fig. 5(b)
 327 further revealed the closeness between the simulation and experimental results of the $I-V$
 328 data.



329

330 **Fig. 5. Simulation (calculated) and experimental (measured) currents for single-diode**
331 **model of R.T.C. France solar cell (a) and their I - V curves (b).**

332

333 The accuracy of simulated I - V data were compared to those reported in the literature.
334 It was found that BA outperformed several recently reported methods as depicted in Table 1,
335 wherein the uncertainty percentage in the extracted parameters is also given. Additionally, the
336 extracted parameters of R.T.C. France solar cell using the proposed technique were compared
337 to those determined by some of other reported methods. The error between simulation and
338 experimental I - V data in terms of SAE, MAE and RMSE indicated an excellent accuracy for
339 the proposed BA which was attributed to the strong reliance of accurate determination of the
340 PV cells and modules parameters. In short, the proposed approach achieved lowest RMSE
341 value of $(7.7896 \pm 0.005\%) \times 10^{-4}$ for the R.T.C. France solar cell, which was lower than those
342 obtained by the existing state of the art techniques such as PGJAYA, ILCOA, HFAPS and
343 ER-WCA.

344

345 **Table 1. Comparison of different parameter extraction methods for single-diode model**
346 **of R.T.C. France solar cell worked at 33 °C and 1000 W/m².**

Method	n	R_s (Ω)	R_{sh} (Ω)	I_L (A)	I_o (μ A)	SAE	MAE	RMSE
BA (proposed)	1.4732	0.0367 \pm 0.002%	52.4722	0.7608 \pm 0.004%	0.2983 \pm 0.006%	$(1.7789 \pm 0.002\%) \times 10^{-2}$	6.8420 $\times 10^{-4}$	$(7.7896 \pm 0.005\%) \times 10^{-4}$
PGJAYA (Yu et al., 2019)	1.4812	0.0364	53.7185	0.7608	0.3230	NA	NA	9.8602 $\times 10^{-4}$
ILCOA (Pourmoussa et al., 2019)	1.4811	0.0364	53.7187	0.7608	0.3230	NA	NA	9.8602 $\times 10^{-4}$
HFAPS (Beigi and Maroosi, 2018)	1.4811	0.0364	53.6784	0.7608	0.3226	NA	NA	9.8602 $\times 10^{-4}$
ER-WCA (Kler et al., 2017)	1.4811	0.0364	53.6910	0.7608	0.3227	NA	6.7985 $\times 10^{-4}$	9.8602 $\times 10^{-4}$
DET (Chellaswamy and Ramesh, 2016)	1.4870	0.0360	54.5320	0.7510	0.3150	NA	NA	9.3000 $\times 10^{-4}$
IJAYA (Yu et al., 2017)	1.4811	0.0364	53.7595	0.7608	0.3228	NA	NA	9.8603 $\times 10^{-4}$
ISCE (Gao et al., 2018)	1.4812	0.0364	53.7185	0.7608	0.3230	1.7704 $\times 10^{-2}$	NA	9.8602 $\times 10^{-4}$
EHA-NMS (Chen, Z. et al., 2016)	1.4812	0.0364	53.7185	0.7608	0.3230	1.7704 $\times 10^{-2}$	NA	9.8602 $\times 10^{-4}$
R _c -IJADE (Gong and Cai, 2013)	1.4812	0.0364	53.7185	0.7608	0.3230	1.7704 $\times 10^{-2}$	NA	9.8602 $\times 10^{-4}$
PCE (Zhang et al., 2016)	1.4811	0.0364	53.7185	0.7608	0.3230	NA	NA	9.8602 $\times 10^{-4}$
ABC (Oliva et al., 2014)	1.4817	0.0364	53.6433	0.7608	0.3251	NA	8.3034 $\times 10^{-4}$	9.8620 $\times 10^{-4}$
GOTLBO (Chen, X. et al., 2016)	1.4838	0.0363	54.1154	0.7608	0.3316	NA	NA	9.8744 $\times 10^{-4}$
CSO (Guo et al.,	1.4812	0.0364	53.7185	0.7608	0.3230	NA	6.7968 $\times 10^{-4}$	9.8602 $\times 10^{-4}$

2016)									
STLBO (Niu et al., 2014)	1.4811	0.0364	53.7187	0.7608	0.3230	NA	8.2900×10^{-4}	9.8602×10^{-4}	
ABC-DE (Hachana et al., 2013)	1.4799	0.0364	53.7185	0.7608	0.3230	NA	NA	9.8602×10^{-4}	
BMO (Askarzadeh and Rezazadeh, 2013b)	1.4817	0.0364	53.8716	0.7608	0.3248	NA	4.6210×10^{-3}	9.8608×10^{-4}	
NM-MPSO (Hamid et al., 2016)	1.4812	0.0364	53.7222	0.7608	0.3230	NA	4.5980×10^{-3}	9.8602×10^{-4}	
MABC (Jamadi et al., 2016)	1.4814	0.0364	53.4000	0.7608	0.3213	NA	8.3118×10^{-4}	9.8610×10^{-4}	
GGHS (Askarzadeh and Rezazadeh, 2012)	1.4822	0.0363	53.0647	0.7609	0.3262	NA	4.6000×10^{-3}	9.9097×10^{-4}	
ABSO (Askarzadeh and Rezazadeh, 2013a)	1.4758	0.0366	52.2903	0.7608	0.3062	NA	NA	9.9124×10^{-4}	
IGHS (Askarzadeh and Rezazadeh, 2012)	1.4874	0.0361	53.2845	0.7608	0.3435	NA	NA	9.9306×10^{-4}	
CPSO (Wei et al., 2011)	1.5033	0.0354	59.0120	0.7607	0.4000	NA	1.6800×10^{-1}	1.3900×10^{-4}	
CWOA (Oliva et al., 2017)	1.4812	0.0364	53.7987	0.7608	0.3239	NA	8.2800×10^{-4}	9.8604×10^{-4}	
GA (Jervase et al., 2001)	1.5750	0.0290	42.3730	0.7620	0.8090	NA	NA	1.9100×10^{-2}	

347 NA: not available in the literature

348

349

350

351

352

353

354

355

356

357

358

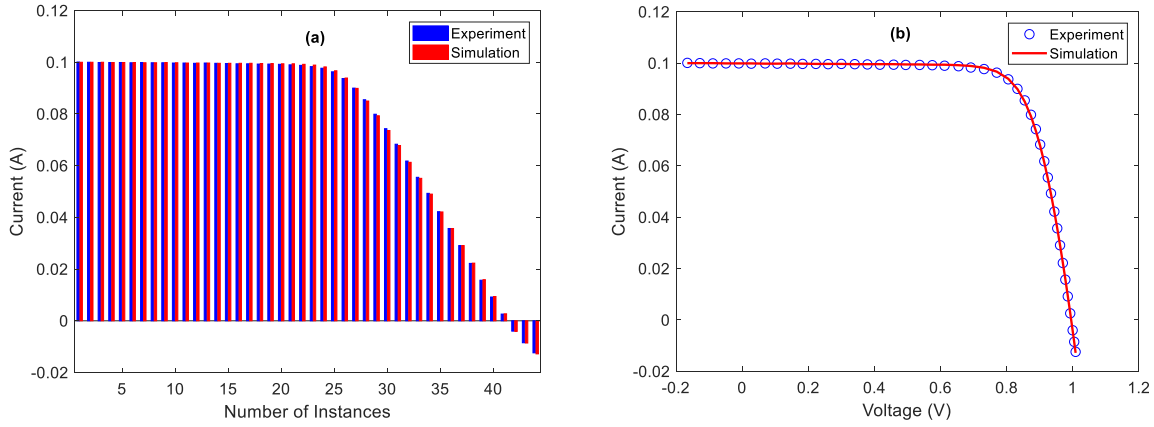
359

360

361

362

Following the earlier procedures, the solar cell parameters of the second PV cell was determined and BA model was validated on PVM 752 GaAs thin film solar cell (Jordehi, 2018). After determining the cell parameters, the simulated currents were compared with the experimental ones (Appendix B). Fig. 6(a) and Fig. 6(b) displays the excellent fit of the simulated data with the measured one, where a trivial deviation around the maximum power point was observed with naked eyes. This might be referred to the effect of the extrapolated method that was applied to identify the values of V_m and I_m . The calculated/simulated $I-V$ data were compared with those reported in the literature. It was concluded that BA performed excellently to determine the PV parameters of the PVM 752 GaAs with lowest RMSE of $(2.1049 \pm 0.007\%) \times 10^{-4}$ (see Table 2), wherein the uncertainty percentage in the extracted parameters is also given. The tiny values of SAE, MAE and RMSE clearly signified excellent competitive accuracy for the proposed method that strongly relied on the accurate determination of PV cells parameters.



363
364
365

Fig. 6. Simulated and experimental currents for single-diode model of PVM 752 GaAs solar cell (a) and their I - V curves (b).

366

367

368

369

370

Table 2. Comparison of different parameter extraction methods for single-diode model of PVM 752 GaAs thin film cell operated at 25 °C and 1000 W/m².

Method	n	R_s (Ω)	R_{sh} (Ω)	I_L (A)	I_o (pA)	SAE	MAE	RMSE
BA (proposed)	1.7341±0.001%	0.6165±0.007%	684.5160	0.0999±0.007%	19.4226	(7.4258±0.008%) ×10 ⁻³	1.6877×10 ⁻⁴	(2.1049±0.007%) ×10 ⁻⁴
ABC (Jordehi, 2018)	1.7742	0.5000	100.0000	0.1033	32.000	NA	NA	2.0412×10 ⁻³
BSA (Jordehi, 2018)	1.8586	0.5000	100.0000	0.1039	84.900	NA	NA	2.1469×10 ⁻³
CPSO (Wei et al., 2011)	1.6171	0.3466	14.2400	0.1165	0.000	NA	NA	2.5400×10 ⁻²
ELPSO (Jordehi, 2018)	1.7686	0.1591	14.4300	0.1150	0.000	NA	NA	2.5400×10 ⁻²

371

372

373

3.2 Validation on PV Modules

374

375

376

377

378

379

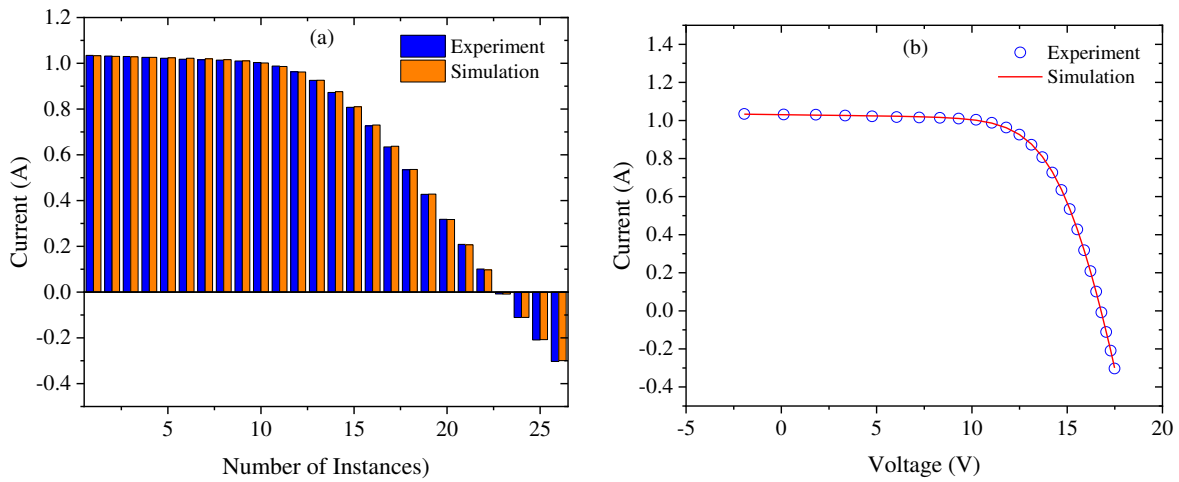
380

381

In addition to PV cells, six different solar modules were also tested under various environmental conditions to extract the parameters and further validation of the proposed BA technique. The first module was Photowatt-PWP201 comprising of 36 polycrystalline silicon cells in series that operated at 45 °C and 1000 W/m². The experimental I - V data of this module was obtained following the earlier work (Easwarakhanthan et al., 1986). The simulated I - V results are depicted in Appendix C, while the extracted parameters along with methods accuracy are summarized in Table 3, wherein the uncertainty percentage in the extracted parameters is also given.

382 Fig. 7 shows the curve fitting results for Photowatt-PWP201 solar module obtained by
383 the proposed method. The calculated currents are shown to tally very well with the measured
384 ones in both high and low voltage regions. With this method of simulation and parameters
385 extraction, a lowest RMSE of $(2.1256 \pm 0.002\%) \times 10^{-3}$ was achieved for Photowatt-PWP201
386 solar module, implying higher accuracy of BA compared to that of several reported methods
387 (Table 3). Moreover, the proposed technique does not require any manual initialization of
388 parameters. Conversely, some optimization problems need to be continuously perturbed
389 through parameters variation, thereby increasing the computational cost and leading to an
390 entrapment in the local optimum.

391



392

393

394

395

Fig. 7. Simulated and experimental currents for single-diode model of Photowatt-

396

PWP201 solar module (a) and their I - V curves (b).

397

398

399

400

401

Table 3. Comparison of various parameter extraction methods for single-diode model of Photowatt-PWP201 solar module comprising 36 polycrystalline silicon cells in series worked at 45 °C and 1000 W/m².

Method	n	R_s (Ω)	R_{sh} (Ω)	I_A (A)	I_o (μ A)	SAE	MAE	RMSE
BA (proposed)	1.3356 \pm 0.006%	1.2184 \pm 0.003%	761.4900	1.0323 \pm 0.003%	2.9983 \pm 0.007%	43.0390 \times 10 ⁻³	(1.6553 \pm 0.004%) \times 10 ⁻³	(2.1256\pm0.002%)\times10⁻³
PGJAYA (Yu et al., 2019)	1.3512	1.2013	981.8545	1.0305	3.4818	NA	NA	2.4250 \times 10 ⁻³
HFAPS (Beigi and Maroosi, 2018)	1.3512	1.2013	984.2813	1.0305	3.4842	NA	NA	2.4251 \times 10 ⁻³
ER-WCA (Kler et al., 2017)	1.3553	1.1963	961.0530	1.0306	3.6146	NA	1.5829 \times 10 ⁻³	2.3558 \times 10 ⁻³
IJAYA (Yu et al., 2017)	1.3508	1.2016	977.3752	1.0305	3.4703	NA	NA	2.4251 \times 10 ⁻³

ISCE (Gao et al., 2018)	1.3512	1.2013	981.9823	1.0305	3.4823	41.7879×10^{-3}	NA	2.4251×10^{-3}
EHA-NMS (Chen, Z. et al., 2016)	1.3512	1.2013	981.9823	1.0305	3.4823	41.7879×10^{-3}	NA	2.4250×10^{-3}
MPCOA (Yuan et al., 2014)	1.3474	1.2030	849.6927	1.0319	3.3737	21.5100×10^{-3}	2.6100×10^{-3}	2.4250×10^{-3}
Newton (Easwarakhanthan et al., 1986)	1.3458	1.2057	555.5556	1.0318	3.2875	NA	8.3200×10^{-3}	7.8050×10^{-1}
PS (AlRashidi et al., 2011)	1.3414	1.2053	714.2857	1.0313	3.1756	NA	5.3000×10^{-3}	1.1800×10^{-1}
IP (Tong and Pora, 2016)	1.3106	1.2744	715.8240	1.0333	2.3326	NA	1.7600×10^{-3}	NA
GA (AlRashidi et al., 2011)	1.3496	1.1968	555.5560	1.0441	3.4360	15.3479×10^{-2}	8.8800×10^{-3}	NA

402

403

404

The performance of the proposed algorithm assessed by extracting the parameters of a

405

mono-crystalline solar module (LEYBOLD 664 431) and simulating its I - V characteristics.

406

This solar module was obtained from Leybold GmbH., which comprised of 20 series cells

407

and operated at module temperature of 24 °C under outdoor sunlight intensity of 360 W/m².

408

The experimental I - V data was recorded manually via digital multimeters of type VC-

409

920/Voltcraft with error $\pm 0.08\%$ and 1% for the DC voltage and current, respectively, while a

410

potentiometer was utilized as a variable load across the module terminals. As this solar

411

module was tested under outdoor condition, there has been some variations/noises in the

412

practically measured I - V data. The simulated results obtained using BA are summarized in

413

Table 4. The extracted parameters were $n = 1.2688 \pm 0.001\%$, $R_s = 6.3944 \pm 0.005\% \Omega$, $R_{sh} =$

414

1973.35Ω , $I_\lambda = 0.1544 \pm 0.008\% \text{ A}$ and $I_o = 2.5087 \pm 0.008\% \text{ nA}$. The BA revealed

415

outstanding performance with a lowest RMSE value of $(8.3838 \pm 0.007\%) \times 10^{-4}$.

416

417

Table 4. Calculated/simulated results of BA for single-diode model of Leybold Solar Module (LEYBOLD 664 431) comprising of 20 series cells worked at 24 °C and outdoor sunlight intensity of 360 W/m².

418

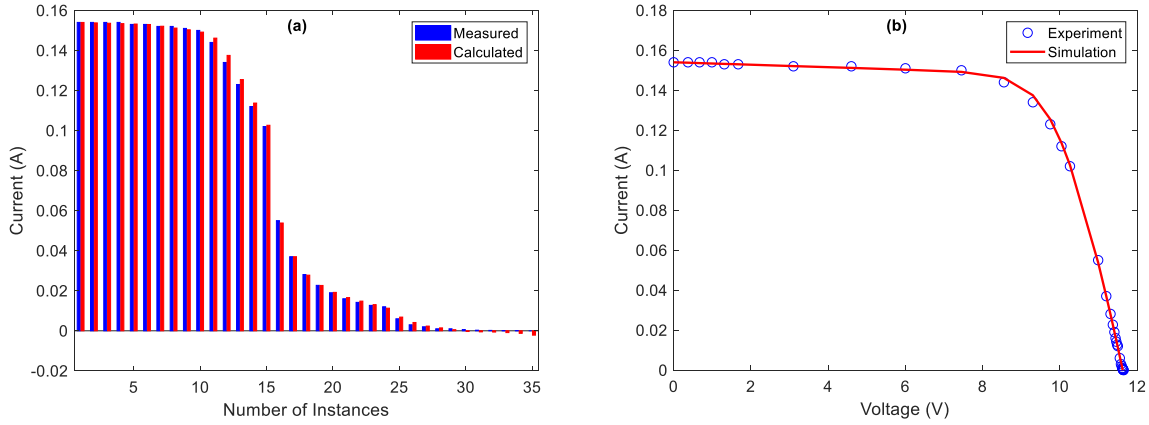
419

Instance	Voltage (V)	Experimental Current (A)	Simulated Current (A)	Absolute Error
1	0.000	0.1540	0.1540	0.0000
2	0.370	0.1540	0.1538	0.0002
3	0.670	0.1540	0.1537	0.0003
4	0.990	0.1540	0.1535	0.0005
5	1.310	0.1530	0.1533	0.0003
6	1.670	0.1530	0.1531	0.0001
7	3.100	0.1520	0.1524	0.0004
8	4.600	0.1520	0.1517	0.0003
9	6.000	0.1510	0.1508	0.0002

10	7.450	0.1500	0.1492	0.0008
11	8.550	0.1440	0.1443	0.0003
12	9.300	0.1340	0.1339	0.0001
13	9.750	0.1230	0.1218	0.0012
14	10.040	0.1120	0.1108	0.0012
15	10.260	0.1020	0.1004	0.0016
16	10.990	0.0550	0.0541	0.0009
17	11.200	0.0370	0.0376	0.0006
18	11.310	0.0281	0.0284	0.0003
19	11.370	0.0227	0.0233	0.0006
20	11.410	0.0190	0.0198	0.0008
21	11.440	0.0160	0.0172	0.0012
22	11.460	0.0142	0.0154	0.0012
23	11.480	0.0127	0.0136	0.0009
24	11.500	0.0120	0.0118	0.0002
25	11.550	0.0060	0.0073	0.0013
26	11.580	0.0030	0.0046	0.0016
27	11.600	0.0020	0.0027	0.0007
28	11.610	0.0010	0.0018	0.0008
29	11.620	0.0010	0.0009	0.0001
30	11.630	0.0006	0.0000	0.0006
31	11.632	0.0003	0.0004	0.0001
32	11.633	0.0002	-0.0003	0.0005
33	11.636	0.0001	-0.0002	0.0003
34	11.640	0.0001	-0.0001	0.0002
35	11.650	0.0000	-0.0020	0.0020
	SAE	$(2.4249 \pm 0.001\%) \times 10^{-2}$		
	MAE	$(6.9283 \pm 0.001\%) \times 10^{-4}$		
	RMSE	$(8.3838 \pm 0.007\%) \times 10^{-4}$		

420

421 Fig. 8 shows that the sensitivity of the proposed approach to the maximum power
422 point (MPP) on the I - V curve is more pronounced in solar modules compared to that of the
423 solar cells (Figs. 5 and 6). Noteworthy, a superior extraction of single-diode parameters can
424 be achieved by the proposed BA method compared to the other computational and heuristic
425 algorithms.



426
427
428
429

Fig. 8. Simulated and experimental currents for single-diode model of Leibold Solar

430

Module (LEYBOLD 664 431) (a) and their I - V curves (b).

431

432

433

434

435

436

437

438

439

440

441

442

443

444

445

The third investigated module was a four series cells-based polycrystalline PV module (STE 4/100) purchased from Leybold GmbH. Experimental I - V data of this cell was measured at module temperature of 22 °C under indoor light intensity of 900 W/m². The measured I - V and simulated I - V dataset obtained by the proposed BA along with the possible errors are enlisted in Table 5. Interestingly, the proposed method could effectively model the I - V behaviour of the module with a RMSE of $(3.3392 \pm 0.004\%) \times 10^{-4}$. Consequently, the extracted parameters of this solar module were discerned to be $n = 1.0304$, $R_s = 2.5567 \pm 0.008\% \Omega$, $R_{sh} = 2184.82 \Omega$, $I_\lambda = 0.0264 \pm 0.005\% A$ and $I_o = 0.1298 \pm 0.001\% nA$. For commercial solar modules the estimated R_s presents lumped series resistance which is the total resistance of electrodes, Ohmic contact resistance and bulk resistance of the module active layer.

Table 5. Results of BA for single-diode model of Leybold Solar Module (STE 4/100) comprised of 4 series cells operated at 22 °C under light intensity 900 W/m².

Instance	Voltage (V)	Experimental Current (A)	Simulated Current (A)	Absolute Error
1	0.00	0.0264	0.0264	0.0000
2	0.10	0.0264	0.0264	0.0000

3	0.30	0.0263	0.0263	0.0000
4	0.50	0.0262	0.0262	0.0000
5	0.70	0.0261	0.0261	0.0000
6	0.90	0.0260	0.026	0.0000
7	1.00	0.0259	0.026	0.0001
8	1.10	0.0258	0.0259	0.0001
9	1.20	0.0257	0.0259	0.0002
10	1.30	0.0256	0.0258	0.0002
11	1.40	0.0253	0.0256	0.0003
12	1.50	0.0252	0.0253	0.0001
13	1.60	0.0247	0.0247	0.0000
14	1.70	0.0232	0.0231	0.0001
15	1.80	0.0189	0.0196	0.0007
16	1.90	0.0121	0.0125	0.0004
17	1.95	0.0081	0.0071	0.0010
18	2.00	0.0000	0.0003	0.0003
	SAE	$(3.5644 \pm 0.008\%) \times 10^{-3}$		
	MAE	$(1.9802 \pm 0.007\%) \times 10^{-4}$		
	RMSE	$(3.3392 \pm 0.004\%) \times 10^{-4}$		

446

447 3.3 Modelling using BA under Different Environmental Conditions

448 The performance assessment and validation of the proposed BA at different device
449 temperatures and various solar irradianations were conducted on three commercial solar
450 modules including KC200GT (multi-crystalline), SX3200N (multi-crystalline) and 1STH-
451 235WH (mono-crystalline) wherein the number of series cells (N_s) for these modules were
452 54, 50 and 60, respectively. The experimental I - V data of the modules were retrieved from the
453 previously reported parameters (Kler et al., 2017). The I - V characteristics at standard test
454 condition (STC) together with the module parameters such as photocurrent (I_{phSTC}), open
455 circuit voltage (V_{oc}), reverse saturation current (I_{oSTC}), series resistance (R_{sSTC}), shunt
456 resistance (R_{shSTC}) and temperature coefficients for short circuit current (K_i) were utilized to
457 produce the experimental I - V characteristics at different temperature and irradiation
458 conditions following expressions:

$$459 \quad I_{\lambda} = \frac{G}{G_{STC}} (I_{\lambda_{STC}} + K_i \Delta T) \quad (20)$$

$$I_o = I_{o_{STC}} \left(\frac{T}{T_{STC}} \right)^3 \exp \left(\frac{qE_g}{nk} \left(\frac{1}{T_{STC}} - \frac{1}{T} \right) \right) \quad (21)$$

$$R_{sh} = \frac{G_{STC}}{G} R_{sh_{STC}} \quad (22)$$

$$R_s = R_{s_{STC}} \quad (23)$$

$$V_{oc} = nV_t \ln \frac{I_\lambda}{I_o} \quad (24)$$

$$E_g = E_{g_{STC}} (1 - 0.0002677\Delta T) \quad (25)$$

where G and T are the irradiance and temperature values at which the module need to be modelled. $E_{g_{STC}}$ is the material bandgap at STC and is considered to be $E_{g_{STC}} = 1.12 \text{ eV}$ for silicon cells and $E_{g_{STC}} = 1.6 \text{ eV}$ for triple junction amorphous cells.

468

469 3.3.1 Temperature Analysis

470 In the first assessment, the modules with various cell temperatures of 25 °C, 50 °C
 471 and 75 °C at the fixed irradiance of 1000 W/m² were considered. The parameters extracted by
 472 BA with RMSE values for different module temperatures are summarized in Table 6. Results
 473 revealed that BA model could extract well the devices parameters at different temperatures
 474 with competitive accuracy. The proposed model outperformed the Hybrid Firefly and Pattern
 475 Search Algorithms (Beigi and Maroosi, 2018).

476

477 **Table 6: Extracted parameters by BA for various solar modules operated at irradiance**
 478 **1000 W/m² and different module temperatures.**

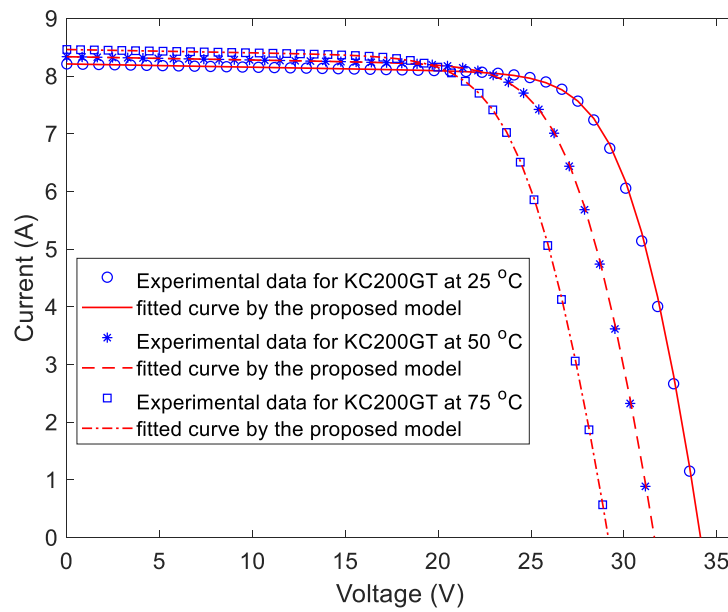
Parameter	KC200GT	SX3200N	1STH-235-WH
$T = 25 \text{ °C}$			
$n (Ns \times n)$	1.1787(63.65)	1.0968(54.84)	1.0900(65.40)
$R_s (\Omega)$	0.2699	0.2818	0.3648
$R_{sh} (\Omega)$	177.506	724.340	1777.600
$I_\lambda (A)$	8.2213	8.9262	8.5394
$I_o (A)$	6.8857×10^{-9}	7.3834×10^{-8}	2.3535×10^{-9}
RMSE	47.6092×10^{-3}	13.1039×10^{-3}	12.9375×10^{-3}

$T = 50\text{ }^{\circ}\text{C}$			
$n (N_s \times n)$	1.1080(59.83)	1.0775(53.87)	1.0982(65.89)
$R_s (\Omega)$	0.3072	0.2902	0.3617
$R_{sh} (\Omega)$	174.963	734.592	1679.890
$I_{\lambda} (\text{A})$	8.3489	9.1513	8.7153
$I_o (\text{A})$	4.5846×10^{-8}	1.4697×10^{-6}	7.2932×10^{-8}
RMSE	24.4609×10^{-3}	8.7261×10^{-3}	14.4952×10^{-3}
$T = 75\text{ }^{\circ}\text{C}$			
$n (N_s \times n)$	1.0949(59.13)	1.0768(53.84)	1.0675(64.05)
$R_s (\Omega)$	0.3114	0.2896	0.3768
$R_{sh} (\Omega)$	175.016	1201.450	1253.930
$I_{\lambda} (\text{A})$	8.4741	9.3724	8.8926
$I_o (\text{A})$	6.0031×10^{-7}	2.5100×10^{-5}	7.3819×10^{-7}
RMSE	12.4216×10^{-3}	6.0655×10^{-3}	3.9505×10^{-3}

479

480 The experimental values and simulated/fitted curves of I - V characteristics for the
481 modules at different cell temperatures are displayed in Figs. 9-11. The fitted I - V curves are
482 shown to be in good agreement with the experimental ones over the entire range of the
483 voltage records. Hence, BA model can be a competitive method to accurately extract the solar
484 cells and modules parameters operating at various environmental conditions. Furthermore, an
485 increase in the solar module's temperature led to an increase in the value of I_{sc} and reduced
486 V_{oc} . The observed increase in I_{sc} with temperature was ascribed to the enhanced charge
487 transport and increased generation current (I_o). Conversely, the reverse trend of V_{oc} change
488 was attributed to the reduced p-n junction ability to separate electrons from holes in the
489 photogenerated pairs. The ideality factor was dropped and approached unity with the rise of
490 temperature, suggesting an improvement in the quality of charge transport within the
491 semiconductor active layer of the devices. Furthermore, the parameters of the
492 monocrystalline based solar module (1STH-235WH) were more sensitive to the temperature
493 change compared to those of the multicrystalline ones (KC200GT and SX3200N). These
494 findings were seen to be in good agreement with theoretical results and experimental

495 observations (Chander et al., 2015; Cuce et al., 2013; Muhammad, Fahmi F. et al., 2017;
496 Radziemska, 2003).

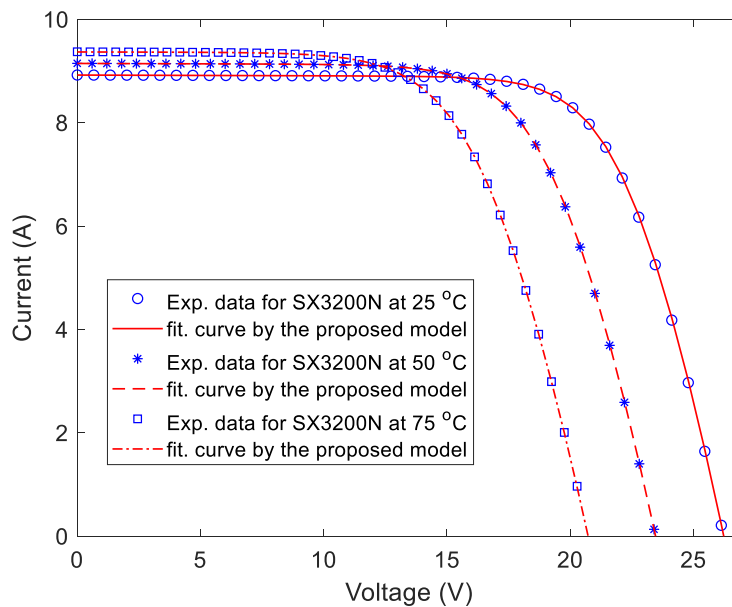


497

498 **Fig. 9. Experimental and simulated I - V characteristics of KC200GT PV module worked**

499

at different temperatures

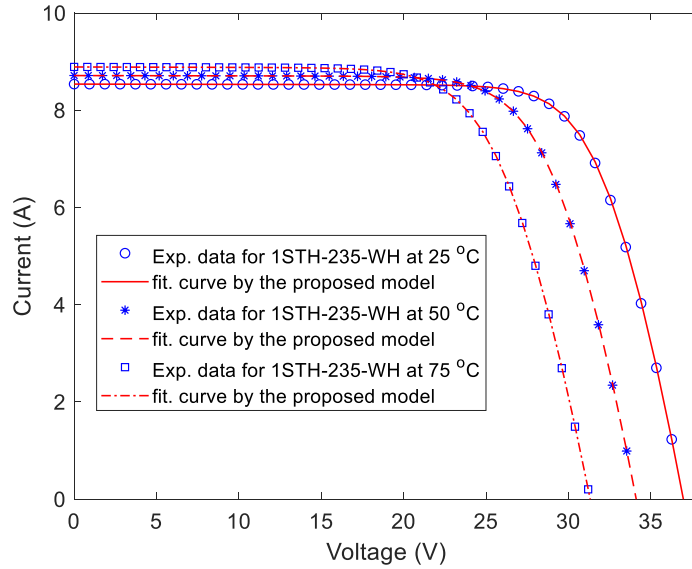


500

501 **Fig. 10. Experimental and simulated I - V characteristics of SX3200N PV module**

502

operated at different temperatures



503

504

Fig. 11. Experimental and simulated I - V characteristics of 1STH-235-WH PV module operated at different temperatures

505

506

507 3.3.2 Irradiation Analysis

508

509

510

511

512

513

514

515

516

517

518

519

520

For the assessment of BA model under various irradiances, the experimental results of the three modules operated at constant temperature of 25 °C and changing irradiances such as 200 W/m², 600 W/m² and 1000 W/m² were considered. Table 7 summarizes the extracted parameters at different irradiances. Results showed that BA could achieve low RMSE when utilized to simulate the I - V characteristics of solar modules at varied irradiances. The comparison between experimental and model results for KC200GT, SX3200N and 1STH-235WH modules is illustrated in Figs. 12, 13, and 14, respectively. It is concluded that the proposed method can be relied on as a competitive model to simulate the I - V characteristics of solar cells and solar modules under different thermal and solar irradiation conditions, thereby extracting the five important parameters of single-diode model. The impact of increased illumination intensity on the PV parameters can be clearly seen, where V_{oc} , I_{sc} and P_m are simultaneously increased with the rise of solar irradiance. The overall trend was the improvement of the solar module's performance upon the rise of irradiation, thereby

521 increasing the photogenerated current. Generally, the values of I_{λ} and I_o were found to
522 enhance and R_s was reduced with the increase of illumination. However, there may be some
523 deviations from these generalizations based on whether the modules are made from
524 monocrystalline or multicrystalline semiconductor. In addition, the existence of some errors
525 that may arise during experimental measurements and accuracy limitations of the proposed
526 models used to import the modules parameters can lead to presence some discrepancies. For
527 instance, experimental findings of Cuce et al. acknowledged that the ideality factor could
528 decrease with the rise of illumination (Cuce et al., 2013). However, the model results
529 displayed a reverse trend for the monocrystalline module (1STH-235WH), where the value of
530 n was observed to increase with the increase of irradiance from 200 to 1000 W/m².

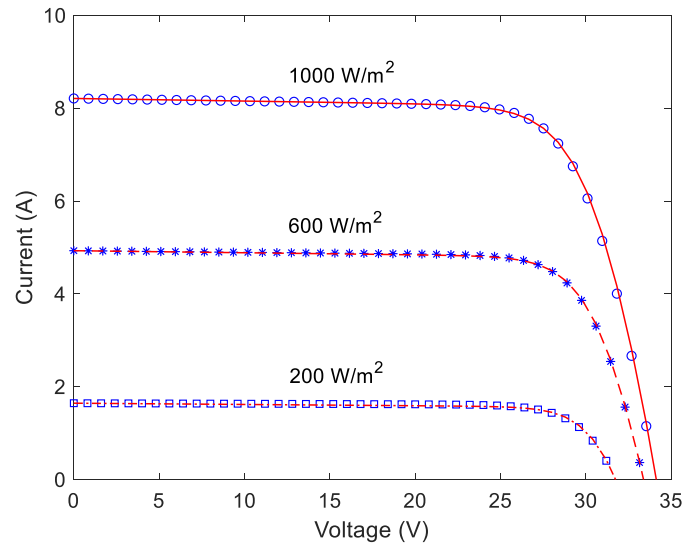
531

532 **Table 7: Extracted parameters from BA for various solar modules operated at 25 °C**
533 **and different solar irradiances.**

Parameter	KC200GT	SX3200N	1STH-235-WH
$G = 1000$			
W/m²			
n ($Ns \times n$)	1.1787(63.65)	1.0968(54.84)	1.0900(65.40)
R_s (Ω)	0.2699	0.2818	0.3648
R_{sh} (Ω)	177.506	724.340	1777.600
I_{λ} (A)	8.2213	8.9262	8.5394
I_o (A)	6.8857×10^{-9}	7.3834×10^{-8}	2.3535×10^{-9}
RMSE	47.6092×10^{-3}	13.1039×10^{-3}	12.9375
$G = 600$ W/m²			
n ($Ns \times n$)	1.0215(55.16)	1.1077(55.38)	0.9935(59.61)
R_s (Ω)	0.3285	0.2648	0.3911
R_{sh} (Ω)	225.533	1159.660	461.124
I_{λ} (A)	4.9365	5.3563	5.1291
I_o (A)	2.8012×10^{-10}	8.5715×10^{-8}	2.7885×10^{-10}
RMSE	16.7598×10^{-3}	18.1553×10^{-3}	25.1033×10^{-3}
$G = 200$ W/m²			
n ($Ns \times n$)	0.8851(47.79)	1.0047(50.24)	0.8473(50.84)
R_s (Ω)	0.4195	0.3264	0.5758
R_{sh} (Ω)	364.442	1094.700	690.779
I_{λ} (A)	1.6464	1.7861	1.7098
I_o (A)	9.0884×10^{-12}	1.4427×10^{-8}	6.4094×10^{-12}

RMSE	21.5324×10^{-3}	5.3443×10^{-3}	18.0056×10^{-3}
------	--------------------------	-------------------------	--------------------------

534

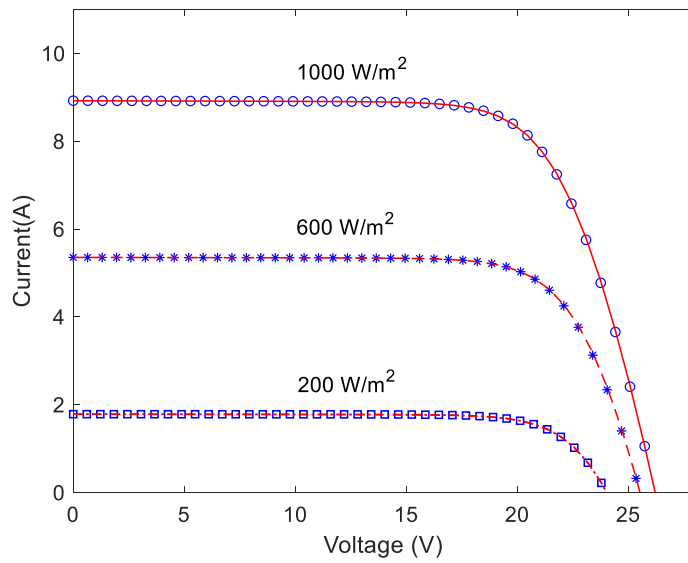


535

536

Fig. 12. Experimental (data points) and simulated (fitted curves) I - V characteristics of KC200GT PV module at different irradiances.

537

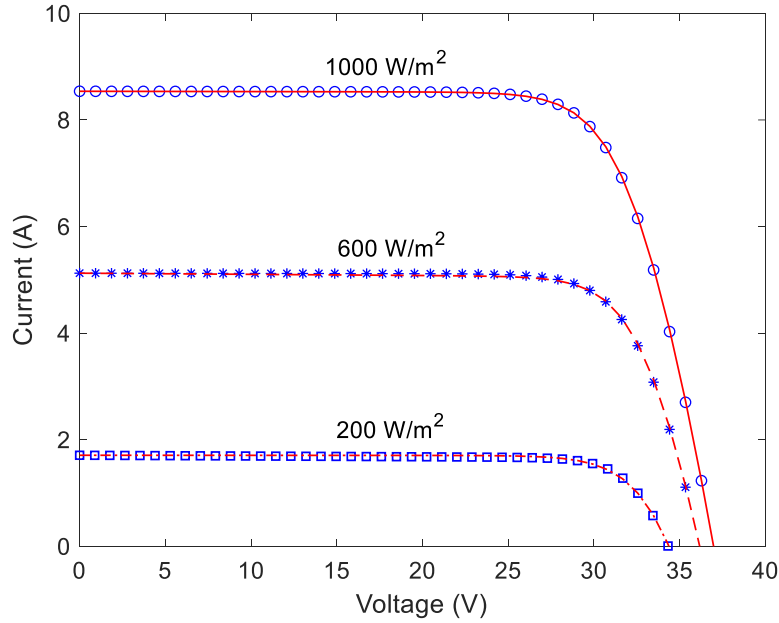


538

539

Fig. 13. Experimental (data points) and simulated (fitted curves) I - V characteristics of SX3200N PV module at different irradiances.

540



541

542 **Fig. 14. Experimental (data points) and simulated (fitted curves) I - V characteristics of**
 543 **1STH-235-WH PV module at different irradiances.**

544

545

546 3.4 Sensitivity analysis and convergence speed

547 The algorithms used to extract solar cells and modules parameters are usually
 548 sensitive to some initializations and fitting parameters. Our proposed BA based algorithm
 549 utilizes a set of I - V data, in which the four PV parameters, V_{oc} , I_{sc} , V_m and I_m , are initially
 550 deduced by curve fitting, then they are used to extract the five PV cells/modules parameters.
 551 It was found that polynomial and Fourier curve fittings are well adopted to find each of V_{oc}
 552 and I_{sc} , respectively. However, we noticed that by changing the fitting type around P_m to
 553 extract V_m and I_m , it is possible to better compensate for efficient extraction of the
 554 cells/modules parameters. Table 8 presents the results of different fitting types that were used
 555 around P_m for the R.T.C. France solar cell and Photowatt-PWP-201 solar module. One can
 556 notice that the polynomial curve fitting has contributed to the lowest RMSE of parameters
 557 extraction for both of the PV devices. Consequently, the second-degree polynomial curve

558 fitting was assigned to extract V_m and I_m for all the datasets investigated by the proposed
559 algorithm.

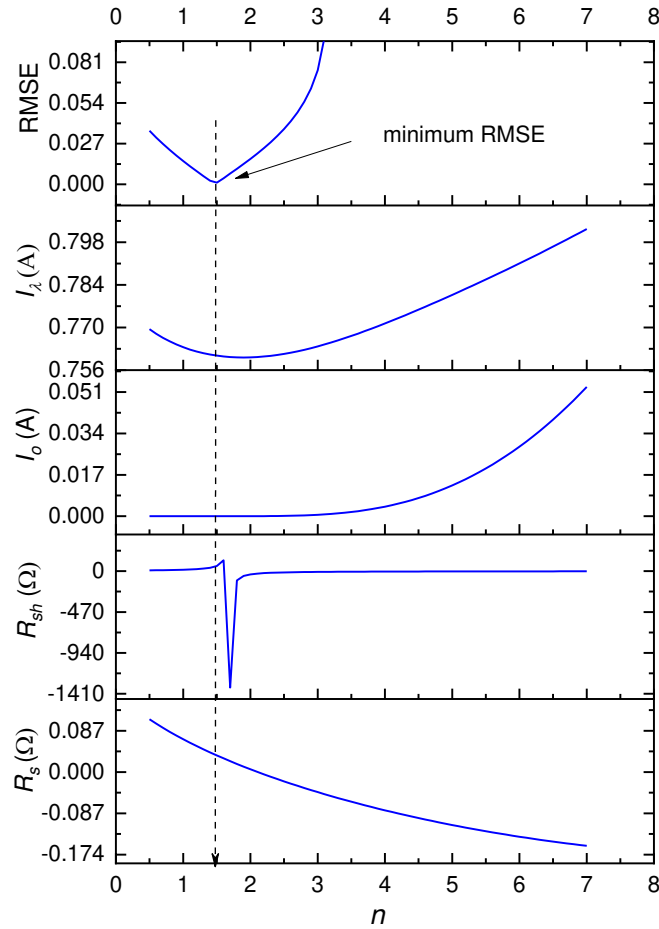
560

561 **Table 8. Utilization of different fitting types around P_m to show their effect on the**
562 **efficiency of extracted PV cells and modules parameters.**

	Fitting type	n	R_s (Ω)	R_{sh} (Ω)	I_λ (A)	I_o (μ A)	RMSE
R.T.C.France solar cell	Gaussian	1.4630	0.0370	49.7426	0.7608	0.2690	8.2130×10^{-4}
	Polynomial	1.4732	0.0367	52.4722	0.7608	0.2983	7.7897×10^{-4}
	Spline	1.4690	0.0368	51.4048	0.7609	0.2866	8.7223×10^{-4}
	Fourier	1.4732	0.0367	52.4722	0.7608	0.2983	7.7897×10^{-4}
	Exponential	1.4853	0.0363	55.8511	0.7608	0.3348	1.4048×10^{-3}
	Power series	1.4853	0.0363	55.8511	0.7608	0.3348	1.4048×10^{-3}
	Sine	1.4146	0.0389	40.7110	0.7610	0.1658	5.1541×10^{-3}
Photowatt-PWP201 solar module	Gaussian	1.2905	1.2740	757.1040	1.0324	1.9242	2.2957×10^{-3}
	Polynomial	1.3357	1.2184	761.4900	1.0323	2.9984	2.1256×10^{-3}
	Spline	1.3811	1.2586	14866.10	1.0307	4.6453	6.1884×10^{-3}
	Fourier	1.3633	1.2240	1616.580	1.0314	3.9227	3.4522×10^{-3}
	Exponential	1.3924	1.1917	1791.930	1.0314	5.0988	3.5561×10^{-3}
	Power series	1.3311	1.3584	12254.20	1.0308	2.9250	8.1751×10^{-3}
	Sine	1.3554	1.2364	17.4322	1.0314	3.6504	3.7012×10^{-3}

563

564 Further investigation on the robustness of the proposed algorithm was carried out by
565 changing the value of ideality factor while recording the values of other four parameters and
566 RMSE simultaneously. That is because in our proposed approach, n is considered to be the
567 only independent variable in Eq. (16), while the other four parameters are dependent on n .
568 For instance, by giving a specific value to n , each of the R_s , R_{sh} , I_o and I_λ can be determined,
569 respectively. Therefore, results of parameters extraction can be highly sensitive to the value
570 of n . Consequently, it is imperative to initialize a range of n values with high decimals, by
571 which the extraction of accurate parameters is guaranteed. It can be observed from Fig. 15
572 that there exists a unique minimum RMSE at which the parameters can be efficiently
573 extracted. The intersection points of the curves with the vertical line passing through the
574 lowest RMSE present the values of the parameters accordingly.



575

576 **Fig. 15. Dependency of the parameters on n while extracting their values at lowest**
 577 **RMSE.**

578

579 The sensitivity of the proposed algorithm to the percentage change in the PV
 580 cells/modules parameters was also analyzed by adding a relative error to each parameter from
 581 10% to -10% in steps of 1% while keeping the other parameters constant. Table 9 shows the
 582 variation in RMSE between the measured and calculated currents for the R.T.C. France solar
 583 cell and Photowatt-PWP-201 solar module as a result of the error inclusion, while the number
 584 inside parenthesis presents the value of the corresponding parameter. Noticeably, the
 585 proposed method is more sensitive to the deviation in the values of n and R_s , with less
 586 sensitivity to each of I_{λ} , I_o and R_{sh} , respectively. It is worth to mention that by using the

587 proposed technique, the values of n , R_s , I_L and I_o are accurately extracted as the minimum
588 RMSE was found to be located at 0% error of these parameters (Table 9). This extraction
589 accuracy can be due to the consideration of n as the only independent variable in Eq. (16) to
590 extract the rest of parameters, which is in agreement with the results presented in Fig. 15.
591 Although the reduction in the value of R_{sh} has led to minimum RMSE at -2% and -5% of
592 error for the solar cell and module, respectively, the presented errors are considered to be
593 insignificant (≤ 0.05). As such, the proposed BA technique is capable of well extracting R_{sh}
594 with trivially above the value at which RMSE is minimal. Consequently, a higher accurate
595 value of R_{sh} can be deduced considering $R_{sh}(1-0.02)$ and $R_{sh}(1-0.05)$ for the solar cells and
596 modules, respectively.

597

598 **Table 9. Variation in RMSE when a systematic relative error of $\pm 10\%$ is presented to**
599 **each of the extracted parameters individually.**

Error (%)	RMSE (Parameter value) for R.T.C. France solar cell					RMSE (Parameter value) for Photowatt-PWP201 solar module				
	n	R_s (Ω)	R_{sh} (Ω)	I_L (A)	I_o (μ A)	n	R_s (Ω)	R_{sh} (Ω)	I_L (A)	I_o (μ A)
10	0.2205 (1.6205)	0.0048 (0.0404)	0.0011 (57.7194)	0.0678 (0.8369)	0.0207 (0.3281)	0.2910 (1.4693)	0.0090 (1.3402)	0.00288 (837.6390)	0.0859 (1.1355)	0.0275 (3.2982)
9	0.2059 (1.6058)	0.0043 (0.0400)	0.0011 (57.1947)	0.0610 (0.8293)	0.0187 (0.3251)	0.2691 (1.4559)	0.0081 (1.3281)	0.00282 (830.0241)	0.0774 (1.1252)	0.0248 (3.2683)
8	0.1898 (1.5911)	0.0038 (0.0396)	0.0010 (56.6700)	0.0543 (0.8217)	0.0166 (0.3223)	0.2457 (1.4426)	0.0073 (1.3159)	0.00275 (822.4092)	0.0689 (1.1149)	0.0221 (3.2383)
7	0.1723 (1.5763)	0.0034 (0.0393)	0.0009 (56.1453)	0.0475 (0.8141)	0.0146 (0.3192)	0.2208 (1.4292)	0.0064 (1.3037)	0.00268 (814.7943)	0.0604 (1.1046)	0.0194 (3.2083)
6	0.1531 (1.5616)	0.0029 (0.0389)	0.0009 (55.6205)	0.0407 (0.8064)	0.0125 (0.3162)	0.1943 (1.4158)	0.0056 (1.2915)	0.00262 (807.1794)	0.0519 (1.0942)	0.0167 (3.1783)
5	0.1323 (1.5469)	0.0024 (0.0385)	0.0009 (55.0958)	0.0340 (0.7988)	0.0105 (0.3132)	0.1662 (1.4025)	0.0048 (1.2793)	0.00260 (799.5645)	0.0434 (1.0839)	0.0139 (3.1483)
4	0.1097 (1.5321)	0.0020 (0.0382)	0.0008 (54.5711)	0.0272 (0.7912)	0.0084 (0.3102)	0.1365 (1.3891)	0.0040 (1.2671)	0.00253 (791.9496)	0.0349 (1.0736)	0.0112 (3.1183)
3	0.0852 (1.5174)	0.0016 (0.0378)	0.0008 (54.0464)	0.0204 (0.7836)	0.0063 (0.3072)	0.1051 (1.3758)	0.0033 (1.2550)	0.00246 (784.3347)	0.0264 (1.0633)	0.0084 (3.0884)
2	0.0589 (1.5027)	0.0012 (0.0374)	0.0008 (53.5216)	0.0137 (0.7760)	0.0042 (0.3043)	0.0719 (1.3624)	0.0027 (1.2428)	0.00244 (776.7198)	0.0179 (1.0529)	0.0058 (3.0584)
1	0.0305 (1.4879)	0.0009 (0.0371)	0.0008 (52.9969)	0.0069 (0.7684)	0.0022 (0.3013)	0.0371 (1.3491)	0.0024 (1.2306)	0.00233 (769.1049)	0.0094 (1.0426)	0.0033 (3.0284)
0	0.0008 (1.4732)	0.0008 (0.0367)	0.0008 (52.4722)	0.0007 (0.7608)	0.0007 (0.2983)	0.0021 (1.3357)	0.0021 (1.2184)	0.00229 (761.4900)	0.0021 (1.0323)	0.0021 (2.9984)
-1	0.0324 (1.4585)	0.0010 (0.0363)	0.0008 (51.9475)	0.0067 (0.7532)	0.0024 (0.2953)	0.0381 (1.3223)	0.0026 (1.2062)	0.00225 (753.8751)	0.0081 (1.0220)	0.0039 (2.9684)
-2	0.0671 (1.4437)	0.0014 (0.0360)	0.0007 (51.4228)	0.0135 (0.7456)	0.0045 (0.2923)	0.0783 (1.3090)	0.0032 (1.1940)	0.00221 (746.2602)	0.0165 (1.0117)	0.0065 (2.9384)
-3	0.1039 (1.4290)	0.0018 (0.0356)	0.0008 (50.8980)	0.0203 (0.7380)	0.0066 (0.2894)	0.1203 (1.2956)	0.0039 (1.1818)	0.00217 (738.6453)	0.0250 (1.0013)	0.0093 (2.9084)

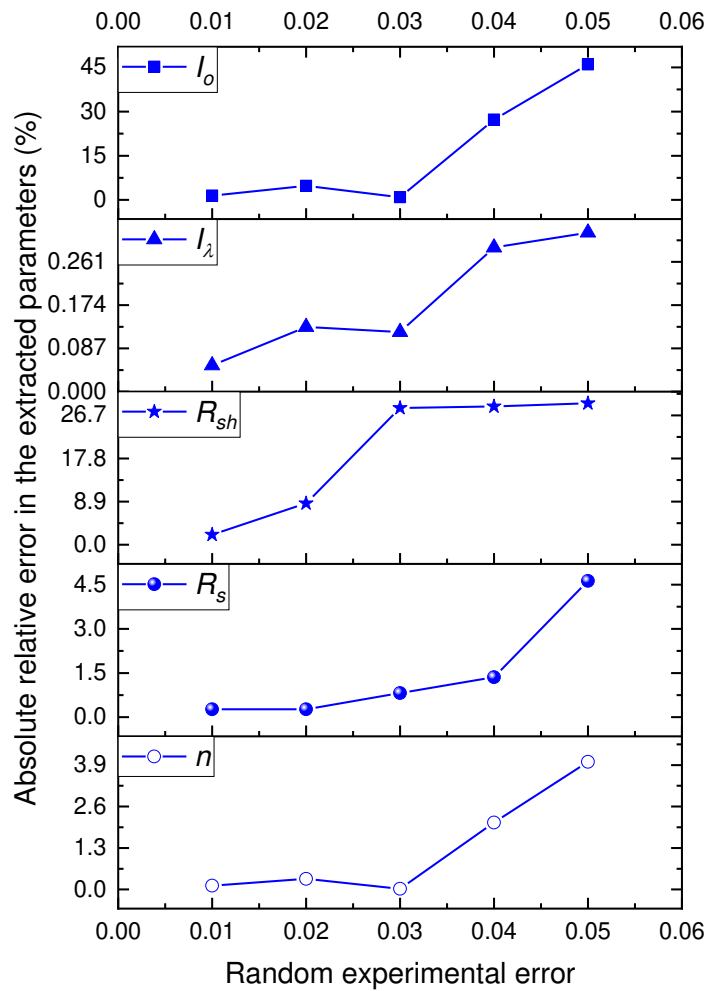
-4	0.1429 (1.4143)	0.0023 (0.0352)	0.0008 (50.3733)	0.0271 (0.7304)	0.0088 (0.2864)	0.1641 (1.2823)	0.0047 (1.1697)	0.00215 (731.0304)	0.0336 (0.9910)	0.0122 (2.8785)
-5	0.1842 (1.3995)	0.0027 (0.0349)	0.0008 (49.8486)	0.0338 (0.7228)	0.0110 (0.2834)	0.2098 (1.2689)	0.0055 (1.1575)	0.00213 (723.4155)	0.0421 (0.9807)	0.0152 (2.8485)
-6	0.2277 (1.3884)	0.0032 (0.0345)	0.0008 (49.3239)	0.0406 (0.7152)	0.0132 (0.2804)	0.2572 (1.2556)	0.0064 (1.1453)	0.00214 (715.8006)	0.0507 (0.9704)	0.0181 (2.8185)
-7	0.2735 (1.3701)	0.0037 (0.0341)	0.0008 (48.7991)	0.0474 (0.7075)	0.0155 (0.2774)	0.3064 (1.2422)	0.0073 (1.1331)	0.00215 (708.1857)	0.0593 (0.9600)	0.0211 (2.7885)
-8	0.3215 (1.3553)	0.0042 (0.0338)	0.0009 (48.2744)	0.0542 (0.7000)	0.0177 (0.2744)	0.3574 (1.2288)	0.0082 (1.1209)	0.00216 (700.5708)	0.0679 (0.9497)	0.0242 (2.7585)
-9	0.3718 (1.3406)	0.0047 (0.0334)	0.0009 (47.7497)	0.0610 (0.6923)	0.0020 (0.2715)	0.4102 (1.2155)	0.0092 (1.1087)	0.00218 (692.9559)	0.0765 (0.9394)	0.0272 (2.7585)
-10	0.4243 (1.3259)	0.0052 (0.0330)	0.0010 (47.2250)	0.0678 (0.6847)	0.0022 (0.2685)	0.4648 (1.2021)	0.0101 (1.0966)	0.00221 (685.3410)	0.0851 (0.9291)	0.0303 (2.6986)

600

601 The presence of noise or error in the measured I - V data is another issue which acts
602 upon reducing the sensitivity of the methods used to extract solar cells and modules
603 parameters. In this context, a random noise with various relative errors was added to the
604 experimental current data of R.T.C. France solar cell, as follows (Zhang et al., 2011):

$$605 \quad I_{with_noise} = I_{without_noise}(1 + percent \times error) \quad (26)$$

606 As such, the noisy data were used to extract device parameters with the proposed BA
607 approach. Fig. 16 shows the percentage of relative error in the extracted parameters for
608 different intensity of the typical random error. It was seen that when the noise relative
609 intensity is 5%, the error for n is about 4%, while for R_s is about 4.6%, suggesting good
610 stability of our proposed BA method under different experimental errors. It is known that
611 calculated current is more sensitive to n , R_s and I_L than R_{sh} and I_o (see Table 9). Therefore, the
612 relatively high percentage error in the extracted I_o and R_{sh} does not affect the validity of our
613 proposed method.



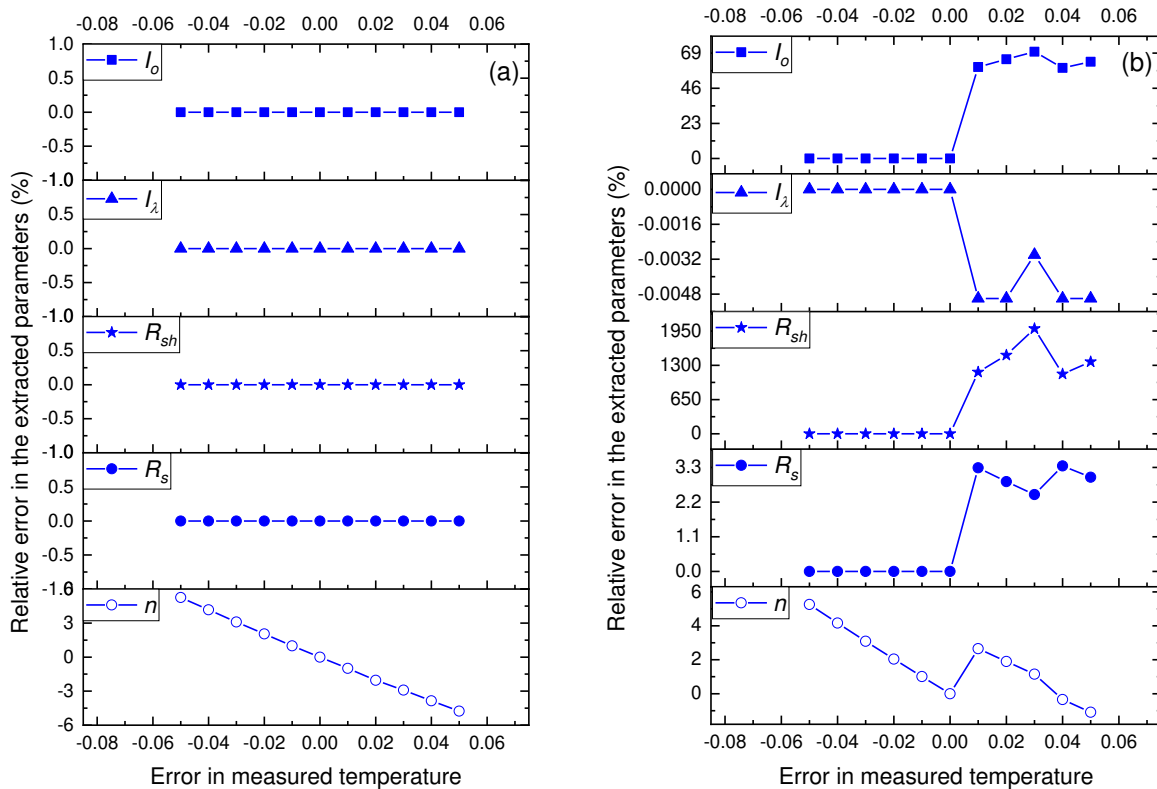
614

615 **Fig. 16. The change in absolute relative error of the extracted parameters when a**
 616 **random error with different relative intensity is added to the experimental data.**

617

618 In addition to the experimental errors arise in the measured I - V , there might be
 619 uncertainties in the measured irradiance and temperature of solar cells/modules. Hence, it is
 620 also interested to observe the impact of errors that are introduced by the outdoor conditions.
 621 Since PV cell temperature (T) is an inherent variable in the equation of single-diode
 622 modelling and presenting itself in almost all the equations, we made further investigations on
 623 the impact of error in the measured temperature on the extracted parameters. Nevertheless, a
 624 relatively linear effect of irradiance error on the deviation of PV cells/modules parameters

625 can be noticed from Eq. (20) to Eq. (24). The change in relative error of the extracted
626 parameters of R.T.C. France solar cell and Photowatt-PWP201 solar module with respect to
627 the errors in measured temperature is shown in Fig. 17. One can notice that for the R.T.C.
628 solar cell, over a broad range of temperature error from -5% to +5%, there exists a zero-
629 relative error for all the extracted parameters except for the ideality factor, of which it is
630 considered insignificant, since error < 5% (see Fig. 17(a)). However, this was seen to be
631 different for the Photowatt-PWP201 solar module, where R_{sh} and I_o have been highly affected
632 by the presence of error in measured T from 1% to 5%. This is where the introduction of a
633 negative error, from -1% to -5%, has led to accurate extraction of R_{sh} and I_o with a zero-
634 relative error. Therefore, it is concluded that the proposed BA method has a high tolerance to
635 the error of measured temperature when it is applied to extract the solar cell parameters. It is
636 worth to mention that PV cell's temperature need to be accurately measured in order to well
637 extracting the device parameters, especially when PV modules are under investigation.



638
639

640

641 **Fig. 17. The change in relative error of the extracted parameters of R.T.C. France solar**
642 **cell (a) and Photowatt-PWP201 solar module (b) against error in the measured**
643 **temperature.**

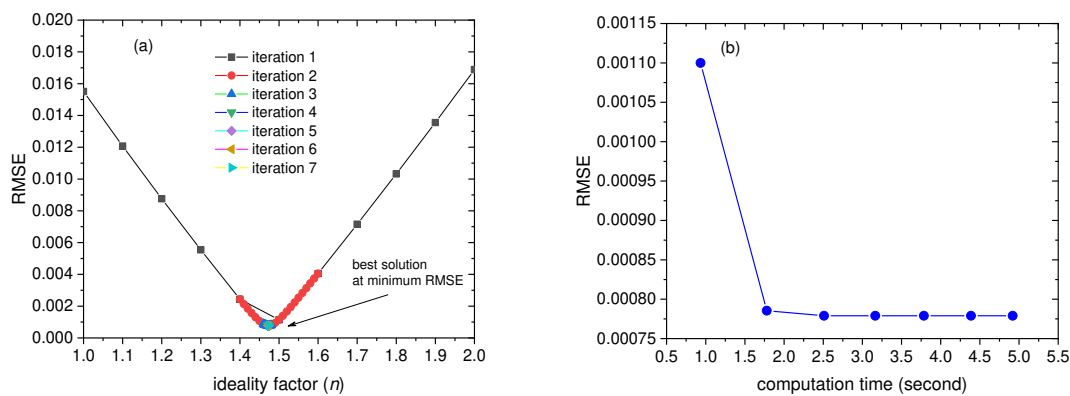
644

645 Interestingly, by using the proposed BA approach, the whole process of parameters
646 extraction takes few seconds. Fig. 18(a) shows that only seven iterations are sufficient to
647 arrive at the best solution with a stable minimum RMSE between the experimental and
648 calculated data. In each iteration, the tuning range of n is narrowed down towards the local
649 minima while maintaining five decimal points for n in the final iteration. It is seen from Fig.
650 18(b) that less than one second is required to complete one iteration and hence the whole
651 computation time is about 5 seconds. This indicates the fast convergence speed for the
652 proposed BA based algorithm, thereby achieving low computational cost yet with high
653 efficiency when it comes to extract the parameters of solar cells and modules parameters.

654 Achieving a right balance between the execution time and accuracy of parameters
655 extraction are considered to be crucial for efficient modelling of solar cells and modules.
656 Very recently, three-diode modelling was proposed as alternatives to the single-diode and
657 double-diode modelling for industrial PV devices (Allam et al., 2016; Khanna et al., 2015). It
658 was however claimed that three-diode model is capable of better interpreting the charge
659 transport and recombination behaviours within the bulk active layer of these devices, the
660 utilized algorithms used for the parameters extraction are time consuming and lose their
661 ability to provide accurate solutions, especially with the increased number of the estimated
662 parameters (Allam et al., 2016). Comparably, the single-diode model is well adopted to
663 rapidly determine the conventional solar cell/module parameters without compromising on
664 efficiency. However, it faces some limitations when it comes to extract the parameters of

665 organic-based, Perovskite and dye-sensitized solar cells (Grätzel, 2003; Muhammad and
 666 Sulaiman, 2011; Snaith et al., 2014). This is because of the non-uniformly distributed series
 667 resistance in these types of PV devices, where interfacial behaviour and nano-phased donor-
 668 acceptor boundaries playing a major role in easily modifying the I - V shape compared to those
 669 of the inorganic solar cells.

670
 671
 672



673
 674
 675

Fig. 18. Minimization of RMSE with the change of n per iteration (a) and computation time required for the whole process of parameters extraction within seven iterations (b).

676
 677

3.5 Comparison with practically measured parameters

678 The proposed BA based method was also applied to extract parameters of blue and
 679 grey solar cells, thereby making a comparison with their practically measured parameters
 680 (Charles et al., 1981) and analytically extracted ones (Cubas et al., 2014b), as shown in Table
 681 10. Noticeably, the extraction results showed great closeness of n , R_s , I_o and I_λ to the
 682 benchmark values. However, the extracted R_{sh} was seen to be trivially higher than that of the
 683 practically measured one. This can be due to the sensitivity characteristic of the proposed BA
 684 based approach which might be originated from the assumption of neglecting $\exp\left(\frac{R_s I_{sc}}{nV_t}\right)$ in
 685 the initially derived equations. Noteworthy, the higher error in the extracted R_{sh} compared to
 686

687 that of the other parameters does not affect the validity of our proposed method as it was
 688 previously demonstrated that calculated current is less sensitive to R_{sh} (see Table 9).

689

690 **Table 10. Comparison of the extracted parameters for blue and grey solar cells**

Device	Method	n	R_s (Ω)	R_{sh} (Ω)	I_L (A)	I_o (A)
Blue SC	BA (proposed)	1.51±0.04	0.066±0.007	1104±15	0.1023±0.0001	(110±10) ×10 ⁻⁹
	Practical/Benchmark (Charles et al., 1981)	1.51±0.07	0.07±0.009	1000±50	0.1023±0.0005	(110±50) ×10 ⁻⁹
	Analytical (Cubas et al., 2014b)	1.51	0.0652	1093	0.1023	111 × 10 ⁻⁹
Grey SC	BA (proposed)	1.72±0.06	0.08±0.01	26.5±0.3	0.5625±0.0002	(5.41±1) ×10 ⁻⁶
	Practical/Benchmark (Charles et al., 1981)	1.72±0.08	0.08±0.01	26±1	0.5625±0.0005	(6±3) ×10 ⁻⁶
	Analytical (Cubas et al., 2014b)	1.72	0.0781	26.25	0.5627	5.4 × 10 ⁻⁶

691

692 4. Conclusions

693 A new approach was used on the single-diode equation for the simple and efficient
 694 extraction of the solar cells and modules parameters, thereby simulation of the $I-V$
 695 characteristics of these devices. This led to the derivation of a non-linear formula for R_s
 696 wherein BA was used to solve. The value of R_s was accurately estimated at every fine-tuned
 697 point of n , which was further used to determine all other devices parameters. The set of
 698 parameters having lowest RMSE value between the experimental and simulated $I-V$ data were
 699 selected to be the best solution. The proposed BA based method was tested and validated on
 700 ten different solar cells and modules under diverse temperatures and irradiations. $I-V$
 701 simulation of R.T.C. France and PVM 752 GaAs solar cell revealed the lowest RMSE value
 702 of 7.79×10^{-4} and 2.11×10^{-4} , respectively. The Photowatt-PWP201, LEYBOLD 664 431 and
 703 STE 4/100 solar modules exhibited the respective RMSE value of 2.13×10^{-3} , 8.38×10^{-4} and
 704 3.34×10^{-4} . The proposed BA model disclosed excellent performance when tested on various
 705 solar modules operated at different cell temperatures and under varied solar irradiations. In
 706 short, it outperformed several previously reported computational and heuristic algorithms

707 used to extract the parameters of single-diode model for solar cells and solar modules under
708 varying environmental conditions.

709

710 **Acknowledgments**

711 The authors sincerely thank the anonymous reviewers for their constructive comments which
712 greatly improved the quality of this paper. The authors should also thank Universiti
713 Teknologi Malaysia for the financial support under Vote No: Q.J090000.21A4.00D20 and
714 Fahmi F. Muhammadsharif thanks Koya University for their administrative support during
715 the implementation of this work.

716

717 **Conflict of Interest**

718 The authors declare that there is no conflict of interest regarding the publication of this work.

719

720 **Appendices**

721 **Appendix A. Simulation results obtained using BA for single-diode model of R.T.C.**
722 **France solar cell worked at 33 °C and irradiation of 1000 W/m².**

723

724

725 **Appendix B. Simulation results obtained via BA for single-diode model of PVM 752**
726 **GaAs thin film cell operated at 25 °C and irradiation of 1000 W/m².**

727

728

729 **Appendix C. Simulation results obtained using BA for single-diode model of Photowatt-**
730 **PWP201 module comprised of 36 polycrystalline silicon cells in series operated at 45 °C**
731 **and 1000 W/m².**

732

733

734 **References**

735 Ahmad, Z., Touati, F., Muhammad, F.F., Najeeb, M.A., Shakoor, R., 2017. Effect of ambient
736 temperature on the efficiency of the PCPDTBT: PC71BM BHJ solar cells. Applied Physics A
737 123(7), 486.

738 Allam, D., Yousri, D., Eteiba, M., 2016. Parameters extraction of the three diode model for
739 the multi-crystalline solar cell/module using Moth-Flame Optimization Algorithm. *Energy*
740 *Conversion and Management* 123, 535-548.

741 AlRashidi, M., AlHajri, M., El-Naggar, K., Al-Othman, A., 2011. A new estimation approach
742 for determining the I–V characteristics of solar cells. *Solar Energy* 85(7), 1543-1550.

743 Askarzadeh, A., dos Santos Coelho, L., 2015. Determination of photovoltaic modules
744 parameters at different operating conditions using a novel bird mating optimizer approach.
745 *Energy Conversion and Management* 89, 608-614.

746 Askarzadeh, A., Rezaadeh, A., 2012. Parameter identification for solar cell models using
747 harmony search-based algorithms. *Solar Energy* 86(11), 3241-3249.

748 Askarzadeh, A., Rezaadeh, A., 2013a. Artificial bee swarm optimization algorithm for
749 parameters identification of solar cell models. *Applied Energy* 102, 943-949.

750 Askarzadeh, A., Rezaadeh, A., 2013b. Extraction of maximum power point in solar cells
751 using bird mating optimizer-based parameters identification approach. *Solar energy* 90, 123-
752 133.

753 Askarzadeh, A., Rezaadeh, A., 2013c. A new heuristic optimization algorithm for modeling
754 of proton exchange membrane fuel cell: bird mating optimizer. *International Journal of*
755 *Energy Research* 37(10), 1196-1204.

756 Bana, S., Saini, R., 2017. Identification of unknown parameters of a single diode photovoltaic
757 model using particle swarm optimization with binary constraints. *Renewable Energy* 101,
758 1299-1310.

759 Beigi, A.M., Maroosi, A., 2018. Parameter identification for solar cells and module using a
760 Hybrid Firefly and Pattern Search Algorithms. *Solar Energy* 171, 435-446.

761 Brent, R.P., 1971. An algorithm with guaranteed convergence for finding a zero of a function.
762 *The Computer Journal* 14(4), 422-425.

763 Brent, R.P., 2013. Algorithms for minimization without derivatives. Courier Corporation.

764 Chaibi, Y., Salhi, M., El-jouni, A., Essadki, A., 2018. A new method to extract the equivalent
765 circuit parameters of a photovoltaic panel. *Solar Energy* 163, 376-386.

766 Chander, S., Purohit, A., Sharma, A., Nehra, S., Dhaka, M., 2015. A study on photovoltaic
767 parameters of mono-crystalline silicon solar cell with cell temperature. *Energy Reports* 1,
768 104-109.

769 Charles, J., Abdelkrim, M., Muoy, Y., Mialhe, P., 1981. A practical method of analysis of the
770 current-voltage characteristics of solar cells. *Solar cells* 4(2), 169-178.

771 Chegaar, M., Ouennoughi, Z., Hoffmann, A., 2001. A new method for evaluating illuminated
772 solar cell parameters. *Solid-state electronics* 45(2), 293-296.

773 Chellaswamy, C., Ramesh, R .2016 ,Parameter extraction of solar cell models based on
774 adaptive differential evolution algorithm. *Renewable Energy* 97, 823-837.

775 Chen, X., Yu, K., Du, W., Zhao, W., Liu, G., 2016. Parameters identification of solar cell
776 models using generalized oppositional teaching learning based optimization. *Energy* 99, 170-
777 180.

778 Chen, Y., Wang, X., Li, D., Hong, R., Shen, H., 2011. Parameters extraction from
779 commercial solar cells I–V characteristics and shunt analysis. *Applied Energy* 88(6), 2239-
780 2244.

781 Chen, Z., Wu, L ,Lin, P., Wu, Y., Cheng, S., 2016. Parameters identification of photovoltaic
782 models using hybrid adaptive Nelder-Mead simplex algorithm based on eagle strategy.
783 *Applied Energy* 182, 47-57.

784 Chin, V.J., Salam, Z., Ishaque, K., 2015. An improved method to estimate the parameters of
785 the single diode model of photovoltaic module using differential evolution, *Electric Power*
786 *and Energy Conversion Systems (EPECS)*, 2015 4th International Conference on. IEEE, pp.
787 1-6.

788 Cubas, J., Pindado, S., de Manuel, C., 2014a. Explicit expressions for solar panel equivalent
789 circuit parameters based on analytical formulation and the Lambert W-function. *Energies*
790 7(7), 4098-4115.

791 Cubas, J., Pindado, S., Victoria, M., 2014b. On the analytical approach for modeling
792 photovoltaic systems behavior. *Journal of power sources* 247, 467-474.

793 Cuce, E., Cuce, P.M., Bali, T., 2013. An experimental analysis of illumination intensity and
794 temperature dependency of photovoltaic cell parameters. *Applied Energy* 111, 374-382.

795 Del Cueto, J., Rummel, S .2005 ,Comparison of diode quality plus other factors in
796 polycrystalline cells and modules from outdoor and indoor measurements, *Conference*
797 *Record of the Thirty-first IEEE Photovoltaic Specialists Conference*, 2005. IEEE, pp. 511-
798 514.

799 Domanski, K., Alharbi, E.A., Hagfeldt, A., Grätzel, M., Tress, W., 2018. Systematic
800 investigation of the impact of operation conditions on the degradation behaviour of
801 perovskite solar cells. *Nature Energy* 3(1), 61.

802 Easwarakhanthan, T., Bottin, J., Bouhouch, I., Boutrif, C .1986 ,Nonlinear minimization
803 algorithm for determining the solar cell parameters with microcomputers. *International*
804 *Journal of Solar Energy* 4(1), 1-12.

805 Gaglia, A.G., Lykoudis, S., Argiriou, A.A., Balaras, C.A., Dialynas, E., 2017. Energy
806 efficiency of PV panels under real outdoor conditions—An experimental assessment in
807 Athens, Greece. *Renewable energy* 101, 236-243.

808 Gao, X., Cui, Y., Hu, J., Xu, G., Wang, Z., Qu, J., Wang, H., 2018. Parameter extraction of
809 solar cell models using improved shuffled complex evolution algorithm. *Energy Conversion
810 and Management* 157, 460-479.

811 Gong, W., Cai, Z., 2013. Parameter extraction of solar cell models using repaired adaptive
812 differential evolution. *Solar Energy* 94, 209-220.

813 Grätzel, M., 2003. Dye-sensitized solar cells. *Journal of photochemistry and photobiology C:
814 Photochemistry Reviews* 4(2), 145-153.

815 Guo, L., Meng, Z., Sun, Y., Wang, L., 2016. Parameter identification and sensitivity analysis
816 of solar cell models with cat swarm optimization algorithm. *Energy conversion and
817 management* 108, 520-528.

818 Hachana, O., Hemsas, K., Tina, G., Ventura, C., 2013. Comparison of different metaheuristic
819 algorithms for parameter identification of photovoltaic cell/module. *Journal of renewable and
820 sustainable energy* 5(5), 053122.

821 Hamid, N.F.A., Rahim, N.A., Selvaraj, J., 2016. Solar cell parameters identification using
822 hybrid Nelder-Mead and modified particle swarm optimization. *Journal of Renewable and
823 Sustainable Energy* 8(1), 015502.

824 Hu, X., Zou, Y., Yang, Y., 2016. Greener plug-in hybrid electric vehicles incorporating
825 renewable energy and rapid system optimization. *Energy* 111, 971-980.

826 Humada, A.M., Hojabri, M., Mekhilef, S., Hamada, H.M., 2016. Solar cell parameters
827 extraction based on single and double-diode models: A review. *Renewable and Sustainable
828 Energy Reviews* 56, 494-509.

829 Ishaque, K., Salam, Z., 2011. An improved modeling method to determine the model
830 parameters of photovoltaic (PV) modules using differential evolution (DE). *Solar Energy*
831 85(9), 2349-2359.

832 Jamadi, M., Merrikh-Bayat, F., Bigdeli, M., 2016. Very accurate parameter estimation of
833 single-and double-diode solar cell models using a modified artificial bee colony algorithm.
834 *International Journal of Energy and Environmental Engineering* 7(1), 13-25.

835 Jervase, J.A., Bourdoucen, H., Al-Lawati, A., 2001. Solar cell parameter extraction using
836 genetic algorithms. *Measurement Science and Technology* 12(11), 1922.

837 Jordehi, A.R., 2018. Enhanced leader particle swarm optimisation (ELPSO): An efficient
838 algorithm for parameter estimation of photovoltaic (PV) cells and modules. *Solar Energy*
839 159, 78-87.

840 Khanna, V., Das, B., Bisht, D., Singh, P., 2015. A three diode model for industrial solar cells
841 and estimation of solar cell parameters using PSO algorithm. *Renewable Energy* 78, 1.113-05

842 Kler, D., Sharma, P., Banerjee, A., Rana, K., Kumar, V., 2017. PV cell and module efficient
843 parameters estimation using Evaporation Rate based Water Cycle Algorithm. *Swarm and*
844 *Evolutionary Computation* 35, 93-110.

845 Kumar, M., Kumar, A., 2017. An efficient parameters extraction technique of photovoltaic
846 models for performance assessment. *Solar Energy* 158, 192-206.

847 Li, Z.-S., Zhang, G.-Q., Li, D.-M., Zhou, J., Li, L.-J., Li, L.-X., 2007. Application and
848 development of solar energy in building industry and its prospects in China. *Energy Policy*
849 35(8), 4121-4127.

850 Louzazni, M., Aroudam, E.H., 2015. An analytical mathematical modeling to extract the
851 parameters of solar cell from implicit equation to explicit form. *Applied Solar Energy* 51(3),
852 165-171.

853 Ma, T., Yang, H., Lu, L., 2014. Development of a model to simulate the performance
854 characteristics of crystalline silicon photovoltaic modules/strings/arrays. *Solar Energy* 100,
855 31-41.

856 Magrab, E.B., Azarm, S., Balachandran, B., Duncan, J., Herold, K., Walsh, G., 2007. *Engineers guide to MATLAB*. Prentice Hall Press.

858 Maouhoub, N., 2018a. Photovoltaic module parameter estimation using an analytical
859 approach and least squares method. *Journal of Computational Electronics*.

860 Maouhoub, N., 2018b. Photovoltaic module parameter estimation using an analytical
861 approach and least squares method. *Journal of Computational Electronics*, 1-7.

862 McEvoy, A.J., Castaner, L., Markvart, T., 2012. *Solar cells: materials, manufacture and*
863 *operation*. Academic Press.

864 Meneses-Rodríguez, D., Horley, P.P., Gonzalez-Hernandez, J., Vorobiev, Y.V., Gorley, P.N.,
865 2005. Photovoltaic solar cells performance at elevated temperatures. *Solar energy* 78(2), 243-
866 250.

867 Muhammad, F.F., Ketuly, K.A., Yahya, M.Y., 2018. Effect of Thermal Annealing on a
868 Ternary Organic Solar Cell Incorporating Gaq3 Organometallic as a Boosting Acceptor.
869 *Journal of Inorganic and Organometallic Polymers and Materials* 28(1), 102-109.

870 Muhammad, F.F., Sulaiman, K., 2011. Photovoltaic performance of organic solar cells based
871 on DH6T/PCBM thin film active layers. *Thin Solid Films* 519(15), 5230-5233.

872 Muhammad, F.F., Sulaiman, K., 2018. Thermal Stability and Reproducibility Enhancement
873 of Organic Solar Cells by Tris (hydroxyquinoline) gallium Dopant Forming a Dual Acceptor
874 Active Layer .*ARO-THE SCIENTIFIC JOURNAL OF KOYA UNIVERSITY* 6(2), 69-78.

875 Muhammad, F.F., Yahya, M.Y., Hameed, S.S., Aziz, F., Sulaiman, K., Rasheed, M.A.,
876 Ahmad, Z., 2017. Employment of single-diode model to elucidate the variations in
877 photovoltaic parameters under different electrical and thermal conditions. *PLoS ONE* 12(8),
878 e0182925.

879 Muhammad, F.F., Yahya, M.Y., Sulaiman, K., 2017. Improving the performance of solution-
880 processed organic solar cells by incorporating small molecule acceptors into a ternary bulk
881 heterojunction based on DH6T: Mq3: PCBM (M= Ga, Al). *Materials Chemistry and Physics*
882 188, 86-94.

883 Müller, B., Hardt, L., Armbruster, A., Kiefer, K., Reise, C., 2016. Yield predictions for
884 photovoltaic power plants: empirical validation, recent advances and remaining uncertainties.
885 *Progress in Photovoltaics: Research and Applications* 24(4), 570-583.

886 Neubauer, C., Samieipour, A., Oueslati, S., Danilson, M., Meissner, D., 2019. Ageing of
887 kesterite solar cells 1: Degradation processes and their influence on solar cell parameters.
888 *Thin Solid Films* 669, 595-599.

889 Niu, Q., Zhang, H., Li, K., 2014. An improved TLBO with elite strategy for parameters
890 identification of PEM fuel cell and solar cell models. *International journal of hydrogen*
891 *energy* 39(8), 3837-3854.

892 Nunes, H ,.Pombo, J., Mariano, S., Calado, M., de Souza, J.F., 2018. A new high
893 performance method for determining the parameters of PV cells and modules based on
894 guaranteed convergence particle swarm optimization. *Applied Energy* 211, 774-791.

895 Oliva, D., Cuevas, E ,.Pajares, G., 2014. Parameter identification of solar cells using artificial
896 bee colony optimization. *Energy* 72, 93-102.

897 Oliva, D., El Aziz, M.A., Hassanien, A.E., 2017. Parameter estimation of photovoltaic cells
898 using an improved chaotic whale optimization algorithm. *Applied Energy* 200, 141-154.

899 Orioli, A., Di Gangi, A., 2016. A criterion for rating the usability and accuracy of the one-
900 diode models for photovoltaic modules. *Energies* 9(6), 427.

901 Otte, K., Makhova, L., Braun, A., Kononov, I., 2006. Flexible Cu (In, Ga) Se₂ thin-film
902 solar cells for space application. *Thin Solid Films* 511, 613-622.

903 Park, J.-Y., Choi, S.-J., 2015. A novel datasheet-based parameter extraction method for a
904 single-diode photovoltaic array model. *Solar Energy* 122, 1235-1244.

905 Pindado, S., Cubas, J., 2017. Simple mathematical approach to solar cell/panel behavior
906 based on datasheet information. *Renewable energy* 103, 729-738.

907 Pourmousa, N., Ebrahimi, S.M., Malekzadeh, M., Alizadeh, M., 2019. Parameter estimation
908 of photovoltaic cells using improved Lozi map based chaotic optimization Algorithm. *Solar*
909 *Energy* 180, 180-191.

910 Radziemska, E., 2003. The effect of temperature on the power drop in crystalline silicon solar
911 cells. *Renewable energy* 28(1), 1-12.

912 Rasool, F., Driberg, M., Badruddin, N., Singh, B.S.M., 2017. PV panel modeling with
913 improved parameter extraction technique. *Solar Energy* 153, 519-530.

914 Senturk, A., Eke, R., 2017. A new method to simulate photovoltaic performance of
915 crystalline silicon photovoltaic modules based on datasheet values. *Renewable energy* 103,
916 58-69.

917 Snaith, H.J., Abate, A., Ball, J.M., Eperon, G.E., Leijtens, T., Noel, N.K., Stranks, S.D.,
918 Wang, J.T.-W., Wojciechowski, K., Zhang, W., 2014. Anomalous hysteresis in perovskite
919 solar cells. *J. Phys. Chem. Lett* 5(9), 1511-1515.

920 Tajuddin, M., Arif, M., Ayob, S., Salam, Z., 2015. Perturbative methods for maximum power
921 point tracking (MPPT) of photovoltaic (PV) systems: a review. *International Journal of*
922 *Energy Research* 39(9), 1153-1178.

923 Tong, N.T., Pora, W., 2016. A parameter extraction technique exploiting intrinsic properties
924 of solar cells. *Applied energy* 176, 104-115.

925 Verma, D., Nema, S., Shandilya, A., Dash, S.K., 2016. Maximum power point tracking
926 (MPPT) techniques: Recapitulation in solar photovoltaic systems. *Renewable and Sustainable*
927 *Energy Reviews* 54, 1018-1034.

928 Villalva, M.G., Gazoli, J.R., Filho, E.R., 2009. Comprehensive Approach to Modeling and
929 Simulation of Photovoltaic Arrays. *IEEE Transactions on Power Electronics* 24(5), 1198-
930 1208.

931 Villalva, M.G., Gazoli, J.R., Ruppert Filho, E., 2009. Comprehensive approach to modeling
932 and simulation of photovoltaic arrays. *IEEE Transactions on power electronics* 24(5), 1198-
933 1208.

934 Wei, H., Cong, J., Lingyun, X., Deyun, S., 2011. Extracting solar cell model parameters
935 based on chaos particle swarm algorithm, *Electric Information and Control Engineering*
936 (ICEICE), 2011 International Conference on. IEEE, pp. 398-402.

937 Xiao, W., Nazario, G., Wu, H., Zhang, H., Cheng, F., 2017. A neural network based
938 computational model to predict the output power of different types of photovoltaic cells. PloS
939 one 12(9), e0184561.

940 Yadir, S., Benhmida, M., Sidki, M., Assaid, E., Khaidar, M., 2009. New method for
941 extracting the model physical parameters of solar cells using explicit analytic solutions of
942 current-voltage equation, Microelectronics (ICM), 2009 international conference on. IEEE,
943 pp. 390-393.

944 Ye, M., Wang, X., Xu, Y., 2009. Parameter extraction of solar cells using particle swarm
945 optimization. Journal of Applied Physics 10.094502 ,(9)5

946 Yeh, W.-C., 2009. A two-stage discrete particle swarm optimization for the problem of
947 multiple multi-level redundancy allocation in series systems. Expert Systems with
948 Applications 36(5), 9192-9200.

949 Yildiran, N., Tacer, E., 2016. Identification of photovoltaic cell single diode discrete model
950 parameters based on datasheet values. Solar Energy 127, 175-183.

951 Yu, K., Liang, J.J., Qu, B.Y., Chen, X., Wang, H., 2017. Parameters identification of
952 photovoltaic models using an improved JAYA optimization algorithm. Energy Conversion
953 and Management 150, 742-753.

954 Yu, K., Qu, B., Yue, C., Ge, S., Chen, X., Liang, J., 2019. A performance-guided JAYA
955 algorithm for parameters identification of photovoltaic cell and module. Applied Energy 237,
956 241-257.

957 Yuan ,X., Xiang, Y., He, Y., 2014. Parameter extraction of solar cell models using mutative-
958 scale parallel chaos optimization algorithm. Solar Energy 108, 238-251.

959 Zagrouba, M., Sellami, A., Bouaïcha, M., Ksouri, M., 2010. Identification of PV solar cells
960 and modules parameters using the genetic algorithms: Application to maximum power
961 extraction. Solar energy 84(5), 860-866.

962 Zhang, C., Zhang, J., Hao, Y., Lin, Z., Zhu, C., 2011. A simple and efficient solar cell
963 parameter extraction method from a single current-voltage curve. Journal of applied physics
964 110(6), 064504.

965 Zhang, Y., Lin, P., Chen, Z., Cheng, S., 2016. A population classification evolution algorithm
966 for the parameter extraction of solar cell models. International Journal of Photoenergy 2016.
967